Title
LOW FREQUENCY APPLICATIONS OF SUPERCONDUCTING QUANTUM INTERFERENCE DEVICES

Author
Clarke, John.

Publication Date
1972-07-01

To be published in IEEE Trans. on Magnetics, January 1973

LBL-1112
Preprint

LOW FREQUENCY APPLICATIONS OF SUPERCONDUCTING QUANTUM INTERFERENCE DEVICES

John Clarke

July 1972

AEC Contract No. W-7405-eng-48

LBL-1112

DISCLAIMER

To be published in IEEE issue on Cryogenic Devices
January 1973

LBL-1112
Preprint

UNIVERSITY OF CALIFORNIA

Lawrence Berkeley Laboratory
Berkeley, California

AEC Contract No. W-7405-eng-48

LOW FREQUENCY APPLICATIONS OF SUPERCONDUCTING QUANTUM INTERFERENCE DEVICES

John Clarke

July 1972

LOW FREQUENCY APPLICATIONS OF SUPERCONDUCTING QUANTUM INTERFERENCE DEVICES

John Clarke*

Department of Physics, University of California,
and Inorganic Materials Research Division,
Lawrence Berkeley Laboratory, Berkeley, Calif.94720

and

Royal Society Mond Laboratory, Cambridge, England

ABSTRACT

This paper reviews the application of Josephson junctions to the measurement of low frequency magnetic fields and voltages. The relevant ideas of flux quantization and Josephson tunnelling are very briefly reviewed, and the various methods of making Josephson junctions mentioned. The two basic types of magnetic sensor, the DC SQUID and the RF SQUID are described in some detail. Their theory of operation, noise limitations, and application to practical devices are discussed. The resolution of SQUIDS commonly used in an analogue mode is 10^{-4} to 10^{-3} $\Phi_o/\sqrt{Hz}$, where Φ_o is the flux quantum. The basic sensor may be used in conjunction with a flux transformer to measure magnetic fields (with a resolution of 10^{-14} $T/\sqrt{Hz}$), magnetic field gradients (with a resolution of 10^{-12} $T/m/\sqrt{Hz}$), and magnetic susceptibilities. The SQUID may also be used as a voltmeter. The resolution is limited by the Johnson noise developed in the resistance of the low temperature circuit, provided that this resistance is not too large: the upper limit in the liquid He^4 temperature range appears to be a few tens of Ohms.

I. INTRODUCTION

The fundamental aspects of the Josephson Effect [1] have been thoroughly investigated, and are by now well understood. Most of the current work in the field is directed towards applications of the effect. These applications may be divided into four main areas: (i) measurement of low frequency voltages and magnetic fields; (ii) mixing and detection of high frequency electromagnetic radiation; (iii) measurement of the fundamental constant ratio e/h, and maintenance of the standard of emf; (iv) computer elements, for example, memories, and switching and logic circuits. Topic (ii) is described by other writers in these Proceedings; (iii) has been reviewed elsewhere.[2] This article is concerned with topic (i). In Section II we shall briefly review the relevant facts of flux quantization and Josephson tunnelling, and mention the various ways in which Josephson junctions have been made. In Section III, we shall be concerned with the two basic types of magnetic field detector, the DC and RF SQUIDS, and describe the theory of their operation, their use as practical devices, and their noise limitations. Section IV deals with the application of either type of SQUID to the measurement of low frequency magnetic fields, field gradients, susceptibilities, and voltages.

II. SUPERCONDUCTIVITY AND THE JOSEPHSON EFFECTS

When a metal becomes superconducting, some of the free electrons become paired together.[3] These pairs are in a single macroscopic quantum state which may be described by a single-valued wave-function[4] $\psi = |\psi| e^{i\phi}$. The long-range phase coherence of the superconducting state has several consequences, among them flux quantization[4,5] and Josephson tunnelling.[1]

A Flux Quantization

The requirement that ψ be single-valued in a closed superconducting ring is expressed by the Bohr-Sommerfeld condition

$$\oint \bar{p}.d\bar{s} = \oint 2m\bar{v}.d\bar{s} + \oint 2e\bar{A}.d\bar{s} = n\hbar . \qquad (1)$$

In Eq.(1), $\bar{p} = 2m\bar{v} + 2e\bar{A}$ is the canonical pair momentum, m and e are the electron mass and charge, $\bar{v}$ is the pair velocity, $\bar{A}$ is the vector potential, $\hbar$ is Planck's constant, and n is an integer. The term $\oint \bar{v}.d\bar{s}$ is proportional to the supercurrent, which flows in a thin surface layer or penetration depth, λ . If the thickness of the ring is large compared with λ, we may choose the path of integration in a region of zero current so that $\oint \bar{v}.d\bar{s}$ vanishes. The term $\oint \bar{A}.d\bar{s}$ is just the total magnetic flux Φ in the ring, in general consisting of an applied flux, and a screening flux generated by induced supercurrents. Eq.(1) then reduces to the condition

$$\Phi = nh/2e = n\,\Phi_o \quad , \tag{2}$$

which demonstrates that the flux is quantized in units of the flux quantum Φ_o, approximately 2×10^{-15} Wb.

B The Josephson Equations

A second important manifestation of the quantum nature of superconductors is Josephson tunnelling.[1] If two bulk superconductors are separated by a thin insulating barrier they are coupled by an energy[1,6,7]

$$E_c = - I_c\Phi_o/2\pi \quad . \tag{3}$$

Provided E_c is large compared with the thermal fluctuation energy kT, phase coherence extends across the barrier and a time-independent supercurrent may be passed through it up to a maximum value I_c, known as the critical current. The difference between the phases of the two superconductors, $\Delta\phi$, adjusts to the externally applied current I, according to the relation[1,6]

$$I = I_c\sin(\Delta\phi) \quad . \tag{4}$$

If a current greater than I_c is passed through the junction, a voltage V appears across it. The phase difference then evolves with time, and the supercurrent oscillates

at a frequency

$$\nu = (1/2\pi)d(\Delta\phi)/dt = 2eV/h = V/\Phi_o \quad . \qquad (5)$$

C Types of Josephson Junctions

Fig.1 illustrates various types of Josephson junctions. Fig.1(a) shows the "classic" tunnel junction in which Josephson tunnelling was first observed.[7] A narrow film of superconductor is evaporated on to a substrate and oxidized by one of several techniques[8] to a depth of 10 to 20Å. A second evaporated strip across the first completes the junction. Typical resistances are in the range 10^{-3} to 10^{2} Ω at room temperature. Early tunnel junctions were not considered very reproducible or reliable, and other types were developed and used in device work. However, in the last few years, a number of authors[9] have successfully prepared Nb-NbOx-Pb junctions, in which the niobium film is oxidized by a glow discharge. It is reported that these junctions can be produced with predictable characteristics, and that their thermal cycling and storage properties are excellent. The critical current of a Nb-NbOx-Pb junction is almost independent of temperature below 4.2K (the boiling point of liquid He^4 under atmospheric pressure), a notable advantage in device applications. Furthermore, tunnel junctions appear to be less prone to damage from electrical transients than some other junction types that

have been used in devices. The only serious disadvantage of the tunnel junction seems to be its high capacitance ($10^{-10} - 10^{-9}$F), which prevents its use as a high frequency detector. However, it may well be that for relatively low frequency work the tunnel junction will finally emerge as the most reliable type of Josephson junction.

In a similar configuration (Fig.1(b)), the oxide layer is replaced by a relatively thick (~1μm) layer of copper.[10] This type of junction is very reproducible and robust, but because of its very low resistance (~$10^{-6}\Omega$) it is not very useful for device applications.

Other junction types consist of a superconductor of very small cross section linking two bulk superconductors, for example, the Anderson-Dayem[11] bridge (Fig.1(c)). Reliable bridges have been developed by Considori et al.[12] from $NbSe_2$, and by Mercereau and co-workers[13] from anodized Nb. One disadvantage of these structures is the strong temperature-dependence of the critical current. This problem is reduced in bridges which are "weakened" by the presence of a thin normal film[13,14] under the constrictions (Fig.1(d)).

Perhaps the most popular type of junction for device work has been the point contact[15] (Fig.3(e)), which consists of a sharpened point pressed against a block; Nb is the favourite material. Very robust versions which can be recycled repeatedly have been developed.[16] The fact that the critical current usually increases somewhat as the temperature is lowered from 4.2K to 1K is sometimes a drawback in device applications.

Finally, the SLUG [17] consists of a bead of Pb-Sn solder (a superconductor) frozen around a piece of niobium wire (Fig.3(f)). This junction is reasonably robust and recyclable, and is certainly the easiest of all to fabricate. It has the advantage of being self-screening against changes in external magnetic fields.

The junctions shown in Figs.1(c)-(f) have been successfully used in instrumentation by various groups. Long-life of any of them demands care in handling, avoidance of thermal shock, and protection from water vapour. However, the users of these devices have reported that with appropriate precautions, a given device may be used for scores of experiments without significant deterioration in characteristics or performance.

D Current-Voltage Characteristics of Josephson Junctions

Provided that it is weakly coupled[18] (i.e., low critical current), any of the junction types shown in Figs.1(b)-(f) is fairly well characterized by a tunnelling element of the form $I = I_c \sin(\Delta\phi)$, shunted by a resistance R. It is useful to examine the current-voltage (I-V) characteristic of this model (Fig.2(a)). An external current $I(>I_c)$, fed from a high impedance source, flows through the junction according to the equation

$$I = I_c \sin[\Delta\phi(t)] + V(t)/R \quad . \qquad (6)$$

The solution[19] $V = R(I^2 - I_c^2)^{1/2}$ is shown in Fig.2(b), and implies a large contribution from the ac supercurrent to the time-averaged current at non-zero voltages. This contribution arises in the following way. Using Eq.(5), which is strictly valid for all types of junction, we can re-write Eq.(6) in the form $d[\Delta\phi(t)]/dt = 2eR\{I-I_c\sin[\Delta\phi(t)]\}/\hbar$. We see that $\Delta\phi(t)$ increases more slowly in the range $2n\pi \leq \Delta\phi \leq (2n+1)\pi$ than it does in the range $(2n+1)\pi \leq \Delta\phi \leq (2n+2)\pi$, so that the oscillation is non-sinusoidal in time, and the time-average is non-zero. A change in the value of I_c therefore modifies the shape of the I-V characteristic for currents up to several times I_c.

Tunnel junctions are shunted by a capacitance, and exhibit a different behaviour. However, the addition of an appropriate external resistive shunt[20] can make their characteristics appear very similar to those shown in Fig.2(b).

III. SUPERCONDUCTING QUANTUM INTERFERENCE DEVICES (SQUIDS).

The first type of magnetic field sensor consisted of a superconducting ring containing two Josephson junctions, and was known as the DC SQUID. Subsequently, the RF SQUID

was developed, in which a single junction was mounted on a superconducting ring. In this section we shall discuss these devices in some detail, but first we make two comments that are relevant to both devices.

In order to make use of simple models, we shall assume that a ring containing one or two junctions still quantizes magnetic flux. This assumption implies that if an external flux Φ_e is applied to a ring of geometric inductance L containing (say) a single junction, a screening current $\Phi_e/L(<I_c)$ generates an exactly opposing flux. The assumption neglects the effective inductance of the junction[1] which may easily be obtained from Eqs. (4) and (5), $L_J = V/\dot{I} = (\Phi_o/2\pi I_c)\sec[\Delta\phi(t)]$. An alternative statement of the assumption is that we have neglected the term $\oint 2m\bar{v}.d\bar{s}$ in Eq.(1) in the junction. If this term were included, we should find that the <u>fluxoid</u> $\oint [(m/e)\bar{v} + \bar{A}].d\bar{s}$ was quantized in units of Φ_o, whereas the <u>flux</u> was not. This assumption may appear to be a rather drastic one, since L is typically Φ_o/I_c, but the resulting models are simple and the predictions in remarkably good agreement with the experimental results. Ouboter and de Waele[21] and Webb[22] have discussed the DC and RF SQUIDS, taking into account the junction inductance.

In order to use either type of SQUID, the junction(s) must be in the non-zero voltage regime for at least some fraction of a duty cycle. During this time, the resistance

will generate a mean square noise current $\overline{I_N^2} = kT/L$ in the ring, and hence a mean square flux noise $\overline{\Phi_N^2} = kTL$. In order to observe quantum effects, we require $\overline{\Phi_N^2} < (\Phi_o/2)^2$, or

$$L < \Phi_o^2/4kT. \qquad (7)$$

At 4K, Eq. (7) sets an upper limit on L of about 2×10^{-8} H. Because of extraneous noise fed into the device by room temperature sources, the effective noise temperature may be rather higher than the bath temperature, and a value of L appreciably less than 2×10^{-8} is usually chosen: a typical value is 10^{-9}H.

A Double Junction Device (DC SQUID)

Principle of Operation

Jaklevic et al.[23] showed that the critical current of the double junction (Fig. 3(a)) was an oscillatory function of the magnetic flux Φ_e applied at right angles to the plane of the ring, the period being Φ_o (Fig. 3(b)). The effect is usually observed by biasing the junctions at a constant current I_o greater than the maximum critical current. The voltage across the junctions is then also an oscillatory function of Φ_e (see Fig. 3(c)), and we shall derive an approximate expression for the amplitude of the voltage modulation.

A magnetic flux Φ_e applied to the ring (of inductance L) generates a screening current $j = \Phi_e/L$ (we assume flux quantization). As the flux is increased to

$\Phi_o/2$, j increases to $\Phi_o/2L$ (A in Fig. 3(d)). If the flux is increased further, it is energetically favourable for the ring to make a transition from the k = 0 quantum state to the k = 1 state (from A to B in Fig. 3(d)), so that j reverses direction. As Φ_e is increased to Φ_o, j decreases along BC. In the same way, transitions occur at $\Phi_e = (n + 1/2)\Phi_o$, and j oscillates as a function of Φ_e. Now when there is a current j in the ring, the net current through one junction exceeds that through the other by $2|j|$. The critical current of the first junction is exceeded when the current through the second is smaller by $2|j|$. Consequently, the total critical current of the double junction is reduced by $2|j|$. The maximum reduction in critical current occurs when $\Phi_e = (n+ 1/2)\Phi_o$, and is just $\Delta I_c = \Phi_o/L$. This result is exact[15,17,21,24] in the limit $LI_c >> \Phi_o$, but in general ΔI_c is somewhat less than Φ_o/L. For typical devices $LI_c \sim \Phi_o$ (I_c is the critical current of each junction), and $\Delta I_c \simeq \Phi_o/2L$. If the critical currents of the two junctions are unequal, ΔI_c cannot exceed twice the value of the smaller.

The voltage modulation depth is just

$$\Delta V \simeq \Phi_o R/2L, \qquad (8)$$

where R is the resistance of each junction. In practice, ΔI_c is somewhat less than Φ_o/L, but since the dynamic resistance of a junction is somewhat higher than R in the range I_c to $2I_c$, Eq. (8) is a realistic approximation. For R = 5Ω per junction and L = 10^{-9}H we find $\Delta V \simeq 5\mu V$. If we approximate the oscillations by a tiangular pattern, their slope is

$$\partial V/\partial \Phi_e \simeq \pm R/L, \qquad (9)$$

about 5×10^9 V/Wb for the values given above.

The signal power developed when Φ_e (near $(2n+1)\Phi_o/4$) is changed by $\delta\Phi_e$ is just

$$\delta P \simeq (\delta\Phi_e)^2 R/2L^2, \qquad (10)$$

of which one-quarter would be delivered to a matched load, R/2.

Practical Devices

Most practical DC SQUIDS have used point contacts, and two examples are shown in Fig. 4. In Fig. 4(a) the device is made from a split Nb cylinder, the two halves being insulated by Mylar or glass spacers[15,16]. The point contacts may or may not be adjustable from outside the cryostat. In the version[25] shown in Fig. 4(b), two pieces of Nb foil are clamped together, with a thin Mylar spacer between them. The points do not penetrate the top foil but merely press together the two foils; external adjustment of the points is essential. An alternative form of double junction is the SLUG[17]. The solder apparently makes a junction with the Nb wire at only two or three points, and the critical current of the device is an oscillatory function of the current in the Nb wire.

The DC SQUID can be used to measure magnetic field in a digital mode, by counting the number of oscillations which occur when the field is applied. Counting rates of over 2000 quanta/sec have been achieved[26]. For most purposes, the device is used in a negative feedback mode, in which the critical current change arising from a small change

in $\Phi_e (<< \Phi_o)$ is detected, and a nulling flux fed back to the SQUID. A typical circuit[26] is shown in Fig. 5. The junctions are biased at a constant current I_o, and an ac magnetic field at a frequency of perhaps 10 kHz is applied to the SQUID, with a peak-to-peak amplitude $\lesssim \Phi_o/2$. The ac signal developed across the junctions is detected with a lock-in at the fundamental frequency. When the external field is equivalent to exactly $n\Phi_o/2$, the signal from the junctions is at twice the fundamental frequency, and the lock-in output is zero. When the external field is $(n + 1/4)\Phi_o$ or $(n + 3/4)\Phi_o$, the output from the lock-in is a minimum or maximum respectively. The output from the lock-in is therefore an oscillatory function of Φ_e, the period again being Φ_o. In the feedback mode the SQUID is biased at $\Phi_o = n\Phi_o$ or $(n + 1/2)\Phi_o$ (usually the latter, since the turning point is sharper, as indicated in Fig. 3(b)). A small change $\delta\Phi_e$ then produces a signal of amplitude δV_m (proportional to $\delta\Phi_e$) across the SQUID at the fundamental frequency. It can be shown that, apart from a factor close to unity, $\partial V_m/\partial\Phi_e$ has just the value given by Eq. (9), R/L. In the same way, Eq. (10) is a good approximation to the signal power. The lock-in technique circumvents various sources of 1/f noise in the system; for example: changes in the critical current of the device due to small changes in its temperature; drifts in the bias current I_o; drifts in the thermal emfs in the cryostat leads; and 1/f noise in the preamplifier of the lock-in.

The output from the lock-in is amplified and fed back to the SQUID via the field coil. The SQUID is therefore the null-detector in a feedback system, and the exact shape of the critical current

vs magnetic flux curve becomes unimportant. The frequency response of the measurement is often determined by a time-constant outside the feedback loop. For measurements at essentially zero frequency, a time-constant of 1 sec (noise bandwidth of 0.25 Hz) is convenient. However, a frequency response of up to 1 kHz is easily achievable: for higher frequencies, a correspondingly higher sweep frequency is required.

The resolution obtained is typically 10^{-4} to 10^{-3} $\Phi_o/\sqrt{Hz}$ for a SQUID inductance of 10^{-9}H, that is, 2×10^{-13} to 2×10^{-12}T/$\sqrt{Hz}$ for a SQUID area of $10^{-6}m^2$. The corresponding voltage change detected across the junctions is 10^{-9} to 10^{-8}V/$\sqrt{Hz}$.

Noise Limitations

In order to obtain the best possible resolution with a SQUID, it is essential to take stringent precautions against the effects of extraneous noise. Low frequency fluctuations in the earth's field are typically three orders of magnitude above the resolution of a SQUID, and the noise due to electrical machinery is even greater. To screen against these fluctuations, the cryostat is often surrounded by two or more cylinders of Mumetal, while the SQUID and its associated circuitry are surrounded by a superconducting can. Radio stations are another source of noise, and careful filtering of all leads entering the cryostat is usually necessary. Electrostatic discharges, for example induced by the experimenter touching the cryostat, can also be a problem, and can cause junctions to burn out in extreme cases. Another essential precaution is to ensure that the SQUID and its associated wiring are mounted as rigidly as possible, particularly in measurements involving magnetic fields. Minute vibrations in a small field can generate large spurious signals.

If we assume that all extraneous noise has been excluded, the ultimate resolution of a DC SQUID is set either by noise in the device itself, or by noise in the associated electronics. The inherent noise which ultimately limits the resolution of a DC SQUID is a subject which is not yet completely understood. We shall here give a discussion which assumes that the noise current is given by the Nyquist formula.[27] It should be emphasized that the result obtained may represent only a lower limit on

the noise, and that a proper calculation which takes into account the macroscopic quantum nature of the device could possibly yield a higher noise level.

We assume that in the non-zero voltage regime the junctions generate a mean square noise current in the ring $\overline{I_N^2} = 4kTB/(2R)$, and hence a mean square flux noise $L^2\,\overline{I_N^2} = 2L^2kTB/R$, where B is the system bandwidth. The fraction of a flux quantum δ_{DC} that can be resolved with a signal-to-noise ratio of unity is therefore

$$\delta_{DC} = (2L^2kTB/\Phi_o^2R)^{1/2}. \qquad (11)$$

If we take T = 4K, L = 10^{-9}H, and R = 5Ω, we find $\delta_{DC} \simeq 2.5 \times 10^{-6}/\sqrt{\text{Hz}}$.

The SQUID is connected to the input of a room temperature amplifier whose noise temperature is T_N for the source impedance and frequency in question. The mean square noise voltages of the junction and the amplifier add, and the resolution becomes

$$\delta'_{DC} = \left(2L^2k(T + T_N)\,B/\Phi_o^2R\right)^{1/2}. \qquad (12)$$

The noise temperature at the best low-noise preamplifiers (for example, PAR 185) for optimum source resistance and frequency is less than 1K. If proper impedance matching could be achieved by means of a suitable ideal transformer, the noise contribution of the room temperature amplifier would be almost negligible for a DC SQUID in the He^4 temperature range.

It should be noted that the flux noise per unit bandwidth will be unaffected when the SQUID is operated in a feedback loop.

It is apparent that the resolution of 10^{-4} to 10^{-3} $\Phi_o/\sqrt{\text{Hz}}$ achieved with DC SQUIDS is two orders of magnitude poorer than that estimated by Eq. (12). The nature of the limiting noise source is far from clear. It may well be that good impedance matching of the junction to the room

temperature amplifier has never really been achieved. For example, a typical system has used a Triad G-10 transformer to match the junction to a PAR Type A preamplifier. This combination has a noise figure of perhaps 6dB (referred to room temperature), so that the noise temperature is about 900K, a figure which increases δ'_{DC} to about $4 \times 10^{-5}\ \Phi_o/\sqrt{Hz}$. Excess noise generated in the transformer core is another possible limiting factor. The problem of impedance matching to a room temperature amplifier appears to be a major one in many applications of Josephson junctions.

It seems unlikely that extraneous noise sources are a limiting factor in a well-shielded system, particularly if the whole experiment is performed in a screened room. It is conceivable that inherent noise in the device is limiting the resolution, but on the whole this also seems unlikely. One is left with the feeling that the performance of the DC SQUID should be better than the results that have been achieved, and one may perhaps hope for marked improvements in sensitivity.

B Single Junction Devices (RF SQUID)

Principle of Operation

A number of authors have described the operation of the RF SQUID[14,22,28-31]. There appear to be several modes of operation, but we shall describe in detail only the one in which most of the instruments used to date apparently operate. Simmonds and Parker[32] have confirmed several details of the operation in this mode by means of an analogue computer study.

The basic circuit of the RF SQUID is shown in Fig. 6. A ring of inductance L, containing a single junction of resistance R and critical current I_c, is weakly coupled to the coil, L_T, of a tank circuit. An RF current $i_d \sin \omega t$ (where $\omega/2\pi$ is typically 30 MHz) excites the tank circuit at the resonant frequency, which is slightly modified by the presence of the SQUID . The level of the RF drive is adjusted so that the peak current induced in the SQUID just exceeds the critical current I_c. Under these conditions, the peak amplitude of the RF voltage across the tank circuit, V_T, is an oscillatory function of the flux applied to the ring, Φ_e, the period once again being Φ_o. We now discuss in some detail the operation of the device, and derive an expression for the voltage modulation depth across the tank circuit, ΔV_T.

It is instructive to describe first the behaviour of the SQUID in a quasistatic external flux Φ_e. We con-

sider the case $\Phi_o/2 < LI_c < 3\Phi_o/2$, as shown in Fig. 7, and assume that in each quantum state the induced supercurrent perfectly screens Φ_e. As Φ_e is increased, the screening current builds up until the flux reaches the value $\Phi_c = LI_c$, when a transition from the k = 0 state to the k = 1 state occurs. A further increase in Φ_e causes transitions at $\Phi_e = \Phi_c + \Phi_o$, $\Phi_c + 2\Phi_o$, and so on. If the flux is increased to $3\Phi_o/2$ and then reduced again, the ring remains in the k = 1 state until $\Phi_e = \Phi_o - \Phi_c$, at which point the critical current is again exceeded, and the ring makes a transition back to the k = 0 state. In the same way, if Φ_e is lowered to $-3\Phi_o/2$ and then returned to (say) $+\Phi_o/2$, a second hystericis loop will be traced out. The energy dissipated in <u>each</u> loop is given by the area divided by L, and is

$$\Delta E = 2\Phi_o I_c - \Phi_o^2/L. \qquad (13)$$

If $LI_c \simeq \Phi_o$, Eq. (13) reduces to $\Delta E \simeq \Phi_o I_c$. One half of this energy is dissipated during each transition, when the junction is dissipative for a characteristic time $L/R \sim 2 \times 10^{-10}$ sec, for $L = 10^{-9}$H and $R = 5\Omega$. Notice that if $LI_c < \Phi_o/2$, there will be no hysteresis[33] (in this limit, a different mode of operation is possible[13,29]), while if $5\Phi_o/2 > LI_c > 3\Phi_o/2$, there is the possibility of a transition from the k = 0 state to the k = 2 state at $\Phi_e = \Phi_c$. To avoid multiple transitions, one usually chooses I_c to be comparable with or somewhat higher than Φ_o/L, about 2μA for $L = 10^{-9}$H.

We consider next the interaction of the SQUID with the tank circuit[28,32] (Fig. 6). We suppose initially that $\Phi_e = 0$. When i_d is very small, the peak flux applied to the ring, $Mi_T = QMi_d$, never exceeds $\Phi_c = LI_c$ and there is no dissipation in the SQUID ($Q = \omega L_T/R_T$, $M^2 = K^2 L L_T$, and i_T is the peak current in the tank coil). The tank voltage, V_T, is just a linear function of i_d, as shown in Fig. 8. As i_d is increased the peak flux will equal Φ_c when $i_T = LI_c/M$, or $i_d = LI_c/MQ$, at A in Fig. 8. The corresponding peak voltage across the tank circuit is

$$V_T^{(n)} = \frac{\omega L_T L I_c}{M} , \qquad (14)$$

where the suffix (n) indicates $\Phi_e = n\Phi_o$ (in this case with $n = 0$). At this point, the SQUID makes a transition to <u>either</u> the $k = +1$ state <u>or</u> the $k = -1$ state, depending upon the direction of the RF flux, and energy is extracted from the tank circuit. Later in the RF cycle, the SQUID returns to the $k = 0$ state, and more energy is extracted from the tank circuit. In general, the two energy losses from the tank circuit are not equal, but the total loss from both is just ΔE. Because of this loss, the peak flux on the next half cycle does not exceed the critical flux, and a quantum transition does not occur. The tank circuit in fact takes many cycles ($\sim Q$) to recover sufficient energy to induce a further transition: note that this transition may be into either of the $k = +1$ or -1 states.

In practice, the slow build up of the amplitude of the tank voltage after each quantum transition is not observed, even when the recovery takes many RF cycles. The reason is probably because the fractional loss,

$\Delta E/(\frac{1}{2}L_T(LI_c/M)^2) \sim 2K^2$ if $LI_c \sim \Phi_o$, is rather small. In addition, the small voltage spike that occurs in the tank circuit at each quantum transition is not usually visible.

If i_d is now increased, the transitions still occur at the same values of i_T and V_T, but because energy is supplied at a higher rate, the stored energy builds up more rapidly after each transition. Thus transitions occur more frequently. When i_d has been increased to B (Fig. 8), a quantum transition occurs on each positive and negative peak value of the RF cycle. The excess power supplied to the tank circuit at B over that at A is just $2\Delta E\nu$, the power dissipated when two hysteresis loops are traversed in each RF cycle. A further increase in i_d therefore produces a rise in V_T, and the RF flux applied to the SQUID increases from LI_c at B to $(LI_c + \Phi_o)$ at C. At C, transitions from the $k = \pm 1$ to the $k = \pm 2$ states occur. In an analogous way, a whole series of plateaux and risers is observed in the plot of V_T versus i_d. The increase of i_d along each riser (BC etc.) is always just Φ_o/MQ, corresponding to an increase of Φ_o in the flux applied to the SQUID. However, the length of the plateaux δi_d(AB etc.) should decrease for higher order transitions. The increase in power supplied along each riser is $V_T\delta i_d = 2\Delta E\nu$. Since V_T is greater for higher order plateaux, there should be a corresponding drop in δi_d, although this effect is not always observed experimentally. Notice also that the effective Q of the tank circuit falls as i_d is increased along one of the plateaux.

Let us now apply an external flux $\Phi_e = \Phi_o/2$ to the SQUID; in the absence of any RF flux, a circulating

current $\Phi_o/2L$ will be established. Thus on the half-cycle during which the RF flux is in the same direction as Φ_e, the critical RF flux will be reduced to $(LI_c - \Phi_o/2)$, while on the half-cycle during which the RF flux opposes Φ_e the critical flux will be increased to $(LI_c + \Phi_o/2)$. Referring to Fig. 8, we see that the first plateau begins at D at a drive current $(LI_c - \Phi_o/2)/MQ$, and a tank voltage

$$V_T^{(n+\frac{1}{2})} = \omega L L_T (I_c - \Phi_o/2L)/M. \qquad (15)$$

As i_d is increased along DF, only <u>one</u> hysteresis loop is traversed, corresponding to the transition at an RF flux $(LI_c - \Phi_o/2)$. As i_d is increased beyond F, V_T rises to G, the increase in i_d again being Φ_o/MQ. At G, transitions at an RF peak flux $-(LI_c + \Phi_o/2)$ begin. Thus a series of steps and risers is obtained for $\Phi_e = \Phi_o/2$, interlocking those obtained for $\Phi_e = 0$.

As Φ_e is increased from 0 to $\Phi_o/2$, the value of V_T for the first plateau steadily decreases. For $0<\Phi_e<\Phi_o/2$ the first plateau splits into two distinct plateaux, the lower corresponding to the transition from k=0 to k=1 at an RF flux $(LI_c-\Phi_e)$, and the upper to the transition from k=0 to k=-1 at an RF flux $-(LI_c+\Phi_e)$. For the special case $\Phi_e=\Phi_o/2$, the plateaux corresponding to the transitions from k=0 to k=-1 and from k=1 to k=2 occur at the same value of V_T, and so coincide. The plateaux for the higher order transitions are similarly split. For values of Φ_e between $\Phi_o/2$ and $3\Phi_o/2$, the lowest energy state at the SQUID in the absence of RF flux is the k = 1 state. Thus in this region, the first order transitions

induced by the RF flux are from the k = 1 to the k = 0 and 2 states. As Φ_e is increased from $\Phi_o/2$ to Φ_o, V_T increases back to $V_T^{(n)}$.

In an analogous way, as Φ_e is steadily increased, V_T oscillates between $V_T^{(n)}$ and $V_T^{(n+\frac{1}{2})}$, with a period Φ_o. The modulation amplitude is readily obtained by subtracting Eq. (15) from Eq.(14):

$$\Delta V_T = \frac{\omega \Phi_o L_T}{2M} = \frac{\omega \Phi_o}{2K}\left(\frac{L_T}{L}\right)^{\frac{1}{2}}. \qquad (16)$$

For given values of L and L_T, Eq. (16) implies that ΔV_T can be made arbitrarily large by making the coupling coefficient K arbitrarily small. Clearly, K cannot be made so small that the influence of the SQUID on the tank circuit becomes negligible, and we need to find a lower limit for K. Now in order to operate the SQUID, one has to be able to choose a value of i_d which lies on the first plateau for all values of Φ_e. This requirement, that F (Fig. 8) lies to the right of A, or that DF must be greater than DE, sets a lower limit on K. The power dissipated in the SQUID is zero at D, and $\Delta E\nu$ at F; hence $i_d^{(F)} - i_d^{(D)} = 2\Delta E\nu / V_T^{(n+\frac{1}{2})} = 2K^2\Phi_o/\pi M$, where we have used $V_T^{(n+\frac{1}{2})} = \omega L L_T (I_c - \Phi_o/2L)/M = \omega L L_T \Delta E / 2M\Phi_o$ (note that i_d and V_T are peak, rather than rms values). The increase in i_d along DA (or DE) is just $\Phi_o/2MQ$, so that our criterion becomes

$$K^2 Q > \pi/4 . \qquad (17)$$

This result is not quite exact, because in our discussion we have assumed that the SQUID dissipation entirely dominates the behaviour of the tank circuit, and that the dissipation in R_T is negligible. This assumption implies $2I_c\Phi_o\nu >> R_T(L^2I_c^2/M^2)/2$, or $K^2Q >> \pi/2$, if $LI_c \simeq \Phi_o$. However, there appears to be general agreement[14,22,28-32] that the criterion $K^2Q \gtrsim 1$ represents the optimum operating condition. If K^2Q is very much larger than unity, ΔV_T is less than the maximum possible value, and in addition, more noise may be coupled into the SQUID from the external world. If K^2Q is much less than unity, the peak value of the drive current cannot lie on the plateau for all values of Φ_e.

The model of the RF SQUID just described predicts that the plateaux have zero dynamic resistance, but in practice their resistance is non-zero. This behaviour arises from the effects of thermal fluctuations and has been explained recently by Kurkijärvi and Webb[34]. In the absence of thermal fluctuations, the transition from the k = 0 state to the k = 1 state occurs at a precisely defined value of flux ($\Phi_e + \Phi_{RF}$), when the energy barrier between the two states is zero. However, in the presence of thermal fluctuations, the transition has a certain probability of taking place at a lower value of flux. Just to the right of A (Fig. 8), a quantum transition occurs at the peak of the RF flux only once in many RF cycles. The SQUID

therefore makes many attempts at a transition, and the probability of its occurring in any one cycle is small. Just to the left of B, a transition must occur at each peak value of RF flux, so that the probability of its occurring must be unity. To increase the probability of the transition, the peak value of the RF flux must increase slightly. Hence V_T must also increase slightly as i_d is increased from A to B. The thermal fluctuations will also give rise to noise (see below).

If we assume that the oscillations of V_T against Φ_e are triangular, their slope is

$$\partial V_T/\partial \Phi_e = \pm \Delta V_T/(\Phi_o/2) = \pm \omega L_T/M. \tag{18}$$

We can also calculate the signal power. If the slope of the plateau on which the system is biased is $\varepsilon\omega L_T Q$ ($\varepsilon < 1$), the signal power is $(\delta V_T)^2/\varepsilon\omega L_T Q$ or

$$\delta P_T = \frac{\omega(\delta\Phi_e)^2}{\pi\varepsilon L} , \tag{19}$$

where $(\delta\Phi_e)^2$ is the change in external flux, and we have set $K^2Q = \pi/4$. Notice that the power extracted from the SQUID, $\sim \omega(\delta\Phi_e)^2/L$, has been enhanced by a factor of roughly $1/\varepsilon$.

It is clear from Eqs. (16)-(19) that the amplitude of the signal obtained from the tank circuit is proportional to ω, and the question of the highest possible value of ω arises. For $\omega << R/L$, the impedance of the SQUID is dominated by the resistance

of the junction. The SQUID affects the tank circuit by means of dissipation in the junction resistance, as described in detail above. The effect of a steadily increasing Φ_e is to modulate the Q of the tank circuit. Most practical devices usually operate in this way. On the other hand, for $\omega >> R/L$, the impedance of the SQUID is dominated by the inductance. The effect of increasing Φ_e is to modulate the reactance of the SQUID, and hence the resonant frequency of the tank circuit, which is coupled to the ring. The amplitude of the voltage across the tank circuit is therefore again an oscillatory function of Φ_e, with a period Φ_o, but Eqs. (13)-(17) are no longer valid descriptions. A detailed discussion of the mode $\omega > R/L$ is given by Notarys et al.[13] The highest angular frequency for which the dissipative mode is a valid description is therefore expected to be

$$\omega_m \simeq R/L. \qquad (20)$$

We can also understand this result in the following way. If two hysteresis loops are traversed in each RF cycle, four quantum transitions occur, each one occupying a characteristic time L/R. In order to obtain four more or less distinct transitions, we require $4L/R \lesssim (2\pi/\omega)$, a condition which yields an upper value for ω of roughly ω_m. Simmonds and Parker[32] also found $\omega_m \simeq R/L$ in their analogue simulation. It might be noted that $\nu_m \sim R/2\pi L$ is typically 10^9 Hz or higher, so that the instrumentation required for operation at this frequency becomes somewhat more sophisticated.

It is of interest to insert $\omega = \omega_m = R/L$ in Eqs. (16), (18), and (19). We find, using $K^2Q \simeq 1$,

$$\Delta V_T^{(m)} = \frac{\Phi_o R}{2L}\left(\frac{L_T}{M}\right) \simeq \frac{\Phi_o R}{2L}\left(\frac{L_T}{L}\right)^{1/2} Q^{1/2}, \tag{21}$$

$$\frac{\partial V_T^{(m)}}{\partial \Phi_e} \simeq \frac{R}{L}\left(\frac{L_T}{L}\right)^{1/2} Q^{1/2}, \tag{22}$$

and

$$\delta P_T^{(m)} \simeq \frac{(\delta\Phi_e)^2 R}{\pi\varepsilon L^2}. \tag{23}$$

In Eqs. (21) and (22), the results are just those obtained for the DC SQUID, $\Phi_o R/2L$ and R/L respectively, multiplied by a factor $(L_T\ Q/L)^{1/2}$ which represents the tank circuit amplification. Eq. (23) indicates that the power obtainable from the tank circuit is enhanced by a factor of $\sim 1/\varepsilon$ over that obtainable from the DC SQUID.

Practical Devices

We turn now to a discussion of practical devices, circuits, and performance. Fig. 9 illustrates three popular RF SQUID configurations. The point contact device[28] shown in Fig. 9(a) is manufactured from a hollow cylinder of niobium, the whole structure being somewhat more stable mechanically than the two junction device of Fig. 4(a). The tank coil is placed inside the ring. An even more robust version[28,30,31] is shown in Fig. 9(b). The tank coil is placed in one loop, and the field to be measured applied to the other. If the structure is completely symmetric, a uniform field change over the whole device is not detected, so that the effects of extraneous fields are reduced. A further type[14] of RF SQUID (Fig. 9(c)) consists of a thin superconducting film with a weak link (of the type shown in Figs. 1(c) or (d)) evaporated on to a quartz rod 1-2 mm. in diameter. The tank coil is wound on the rod. In a similar configuration (not illustrated), Goodkind and Dundon [35] have used a thin niobium cylinder sputtered on to a quartz rod and then anodized. The film does not appear to have a well-defined junction.

The RF SQUID can be used in a digital mode to count flux quanta, but is more commonly used in an anologue mode. A typical circuit is indicated in Fig. (10) (after Zimmerman[29]). The RF bias is adjusted so that the peak of the drive current lies on the first plateau of Fig. 8 for all values of Φ_e. A small audio frequency flux

($\lesssim \Phi_o/2$) is also applied to the SQUID. The modulated RF voltage across the tank circuit is amplified (usually by an FET amplifier), demodulated and phase sensitively detected at the audio frequency. In the feedback mode, the SQUID is biased at $\Phi_o = n\Phi_o/2$, just as in the case of the DC SQUID. A small change $\delta\Phi_e$ in the external flux then produces a signal of amplitude δV_m across the tank circuit at the fundamental audio frequency. Once again, $\partial V_m/\partial\Phi_e$ is closely equal to $\left|\partial V_T/\partial\Phi_e\right|$: the appropriate factor has been calculated by Giffard *et al.*[30] and yields

$$\partial V_m/\partial\Phi_e = (4/\pi)\left|\partial V_T/\partial\Phi_e\right| = 8\Delta V_T/\pi\Phi_o. \qquad (24)$$

The zero-crossing lock-in technique overcomes various sources of 1/f noise, including slow changes in the critical current, and drifts in the amplitude and frequency of the RF. The output from the lock-in is amplified and fed back to the SQUID, which again acts as a null-sensing device. A dynamic range of $\pm$ 500 Φ_o is typical.[30] Under fully optimized conditions, the maximum slewing rate[30] should be approximately ν_{AF} quanta sec^{-1}, where ν_{AF} is the audio modulation frequency; in practice, somewhat lower slewing rates are achieved.

For the device of Zimmerman et al.[28] the following parameters, which may be taken as typical, are applicable: $L = 4 \times 10^{-10}$H, $L_T = 1.4 \times 10^{-7}$H, $K = 0.2$, $\omega/2\pi = 30$MHz, and $Q \sim 100$. The value of ΔV_T estimated for these parameters is 18μV, in good agreement with the observed value of 14μV. The resolution of the device was approximately $3 \times 10^{-4}\Phi_o/\sqrt{\text{Hz}}$. Sensitivities of 10^{-4} to $10^{-3}\Phi_o/\sqrt{\text{Hz}}$ are generally quoted, corresponding to field resolutions of 2×10^{-13} to 2×10^{-12}T/$\sqrt{\text{Hz}}$ for a SQUID area of 10^{-6} m^2.

Zimmerman and Frederick[36] operated a SQUID at 300MHz, and found that ΔV_T increased by an order of magnitude over that obtained from a 30MHz SQUID, as predicted by Eq. (16). Kamper and Simmonds[37] have constructed a SQUID to operate at 9GHz, and found that ΔV_T approached the value expected from Eq. (16). It seems likely that considerable improvements in signal-to-noise ratio will ultimately be achieved with SQUIDS operated at high frequencies ($\gtrsim R/2\pi L$). Zimmerman[38] has also described an ingenious technique for increasing the resolution of an RF SQUID without going to higher frequencies. He made a fractional turn SQUID, in which twelve loops in parallel were connected across a single point contact. The effective pick-up area of the device was thereby enhanced, whereas the effective inductance was decreased, since the loop inductances are in parallel. By this means the resolution of the device was appreciably improved.

Noise Limitations

As with the DC SQUID, it is of course essential to screen the RF SQUID from extraneous noise sources. We shall discuss in turn the noise contributions of the tank circuit, the amplifier, and the thermal fluctuations in the SQUID.

The tank circuit will generate Johnson noise, the effective resistance being the dynamic resistance of a plateau, $\varepsilon\omega L_T Q$, where ε is the ratio of the slopes of the plateaux and risers. If we take $\varepsilon = 0.1$, $\omega/2\pi = 3 \times 10^7$ Hz, $L_T = 1.4 \times 10^{-7}$H, and $Q = 100$, we find $\varepsilon\omega L_T Q \simeq 250\Omega$. However, it is easily seen that this noise contribution is negligible compared with the noise generated in the FET amplifier connected across the tank circuit. The mean square voltage noise referred to the input of the FET is $\overline{V_N^2} = 4kTrB$, where r is the equivalent noise resistance at room temperature. For a typical device $r \sim 300\ \Omega$ and $\left(\overline{V_N^2}\right)^{1/2} \sim 2\text{nV}/\sqrt{\text{Hz}}$. Since the tank circuit resistance (at 4K or less) is comparable to the FET noise resistance (at room temperature), it is clear that the FET noise is dominant. The flux noise equivalent to this amplifier noise is given from Eq. (24) as $\left(\overline{\Phi_N^2}\right)^{1/2} = \left(\overline{V_N^2}\right)^{1/2} \pi\Phi_o/8\Delta V_T$, from which we obtain

$$\delta_{RF}^{(A)} = \frac{\pi\left(\overline{V_N^2}\right)^{1/2}}{8\ \Delta V_T} . \tag{25}$$

If we take $\left(\overline{V_N^2}\right)^{1/2} = 2\text{nV}/\sqrt{\text{Hz}}$ and $\Delta V_T = 14\mu\text{V}$, we find $\delta_{RF}^{(A)} \simeq 6 \times 10^{-5}/\sqrt{\text{Hz}}$.

As mentioned earlier, thermal fluctuations introduce an uncertainty in the value of the total applied flux at which a quantum transition occurs in the SQUID. The flux noise arising from this uncertainty has

been calculated by Kurkijärvi, and Kurkijärvi and Webb,[34] and may be expressed in the form (subject to certain restrictions)

$$\delta_{RF}^{(KW)} = 3.12 \left(\frac{B}{\nu_{RF}}\right)^{1/2} \frac{LI_c}{\Phi_o}^{1/3} \left(\frac{kT}{\Phi_o}\right)^{2/3} [1 - (\Phi_o/2\pi LI_c)^2]^{1/6} . \qquad (26)$$

If $LI_c = \Phi_o$, Eq. (26) simplifies to $\delta_{RF}^{(KW)} = 3.12(B/\nu_{RF})^{1/2}(LkT/\Phi_o^2)^{2/3}$ $\simeq 3 \times 10^{-5}/\sqrt{Hz}$ for ν_{RF}=30 MHz, $L = 10^{-9}$H, and T = 4K. The total contribution from amplifier noise and SQUID noise is therefore

$$\delta_{RF} = \left[\left(\delta_{RF}^{(A)}\right)^2 + \left(\delta_{RF}^{(KW)}\right)^2\right]^{1/2}, \qquad (27)$$

and for the values given above is approximately $7 \times 10^{-5}/\sqrt{Hz}$. The equivalent flux noise per unit bandwidth remains the same if the SQUID is operated in a feedback circuit.

This theoretical value for the flux resolution is in quite good agreement with the best experimentally determined value of $10^{-4}\ \Phi_o/\sqrt{Hz}$. Giffard *et al.*[30] were able to separate SQUID noise from amplifier noise in their experiment. They found $\delta_{RF}^{(KW)} \simeq (1.0 \pm 0.3) \times 10^{-4}/\sqrt{Hz}$ (with ν_{RF} = 19 MHz); in view of the uncertainties in the values of I_c and L, this result may be regarded as being in quite acceptable agreement with the theoretical prediction. The contribution of the amplifier noise was as expected.

It is noteworthy that an RF SQUID operating at 30 MHz has a performance comparable to or somewhat better than that of a dc SQUID while developing only a few percent ($\sim \omega L/R$) of the signal power. Thus the resonant detection scheme appears to be superior to the techniques

used to measure the critical current of a DC SQUID, probably because of improved impedance matching to the room-temperature amplifier. The high degree of rejection of extraneous noise at frequencies outside the bandwidth of the resonant circuit may also be an important factor.

It appears that RF SQUIDS at RF frequencies of 30 MHz are at the limit of their resolution, approximately $10^{-4}\ \Phi_o/\sqrt{\text{Hz}}$. However, it has already been demonstrated that devices operated at higher frequencies have a correspondingly larger output, and improvements in resolution of at least one order of magnitude should soon be realizable.

IV. APPLICATIONS OF SQUIDS

In the following sections we shall briefly describe the use of SQUIDS to measure magnetic fields, magnetic field gradients, magnetic susceptibilities, and voltages. In principle, either type of SQUID may be used as the sensor. We shall be concerned mostly with circuits in which the SQUID is a null detector in a feedback loop, and we shall assume that the SQUID has a mean square flux noise $\alpha^2\Phi_o^2 B$, where α is (at best) 10^{-4}, and B is the system bandwidth. More detailed accounts of these applications may be found elsewhere;[36,38,39] the article by Giffard _et al._[30] is particularly comprehensive.

A Measurement of Magnetic Field

The SQUID is of course an extremely sensitive magnetometer, with a resolution approaching $10^{-13} T/\sqrt{Hz}$ This high sensitivity implies that the SQUID in an analogue mode is too sensitive for most measurements of field in an open environment. However, in a digital mode, the device may be useful in situations where the direct digital readout is an advantage. An unshielded SQUID may be used directly to make such measurements, or a shielded SQUID may be used in conjunction with the flux transformer described below.

The high sensitivity of the SQUID in an analogue mode means that it is most useful when the magnetic field can be generated in a shielded enclosure. The SQUID can be used directly to measure the field, but it is usually preferable to couple the field by means of a flux transformer. The flux transformer consists of a superconducting loop in the shape shown in Fig.11(a). The loop on the left hand side (area A_2, inductance L_2) is coupled via a mutual inductance $M_2 = \sigma(LL_2)^{1/2}$ to a SQUID operated in the feedback mode shown in either Fig.5 or Fig.10. A magnetic field applied to the right hand loop (area A_1, inductance L_1) generates a supercurrent in the transformer, which in turn produces a flux in the SQUID. The sensitivity of the system will be enhanced if the area of the pick-up loop is larger than that of the secondary loop. The supercurrent generated in the transformer by an applied field δH is $j = \mu_0 \delta H A_1/(L_1+L_2)$. The sensitivity of the system is found by equating the flux applied to the SQUID, $M_2 j$,

to the flux noise of the SQUID, $\alpha\Phi_o B^{1/2}$. The sensitivity is therefore

$$\delta H = \frac{\alpha\Phi_o(L_1+L_2)B^{1/2}}{\mu_o A_1\, \sigma(LL_2)^{1/2}} \quad . \tag{28}$$

We have neglected the stray inductance of the leads connecting the two coils, and also the effect of the transformer inductance in reducing the effective inductance of the SQUID.[38]

If we assume that σ is the same for any configuration of secondary, we can optimize the sensitivity by putting $L_1 = L_2$. Thus the secondary is usually multiturn. The optimized value of Eq.(20) becomes $2\alpha\Phi_o(BL_1/L)^{1/2}/\mu_o A_1\sigma$, and in principle arbitrarily high sensitivity may be achieved by making the pick-up loop sufficiently large. In practice, improvements in sensitivity of about one order of magnitude have been achieved.

B Measurement of Magnetic Field Gradient

The principle of the flux transformer may be extended to measure almost any derivative of the magnetic field. Two examples appear in Figs. 11(b) and (c). In each case, the small secondary loop (which in practice is usually multiturn) and the SQUID coupled to it are shielded by a superconducting can. The two pick-up loops of each gradiometer are wound in such a sense that a uniform magnetic field generates no supercurrent: only field gradients are detected. Using a gradiometer with the configuration of Fig.11(b), Zimmerman and Frederick[36] achieved a sensitivity of 10^{-12}T/m/$\sqrt{\text{Hz}}$.

A difficulty with these gradiometers has been in balancing the two loops with sufficient accuracy. Matching can be achieved in situ if one adjusts the position of a small piece of superconductor inserted in the larger of the two loops.

Gradiometers are particularly useful in an unshielded environment, and are likely to be used extensively in measuring gradients and gradient fluctuations in the earth's field. However, the gradient noise in the earth's field is quite low, so that gradiometers can be used to measure the field gradients generated by nearby sources outside the cryostat. For example, Zimmerman and Frederick[36] have used a gradiometer to take magnetocardiograms.

C Measurement of Magnetic Susceptibility

The magnetometer of Fig.11(a) can be used to measure magnetic susceptibility. The sample is inserted in the pick-up loop, which is usually multiturn, and a uniform magnetic field applied. This configuration is convenient when changes in susceptibility are to be measured. It is often preferable to use the gradiometer assembly of Fig.11(b), with the sample in one of the loops, which is again usually multiturn. If the pick-up coils are properly matched, the uniform background field produces no signal, and only the flux enhancement due to the presence of the sample is detected.

Various applications of this technique have been found. The susceptibility of nuclei at very low temperatures, which varies as $1/T$, has been measured and used in thermometry.[29,30]

Groups at Harvard[40] and Cornell[41] have measured susceptibility fluctuations in superconductors near the transition temperature, while Mercereau and co-workers have measured the susceptibility of biochemical samples over a wide-temperature range.[42] Yet another potential application is to rock-magnetometry.

D Measurement of Voltage

SQUIDS and SLUGS[17] have been widely used as voltmeters. The SQUID is coupled via a mutual inductance $M = \sigma(LL_2)^{1/2}$ to a superconducting coil of inductance L_2, which is in series with a standard resistor R_s and an unknown voltage V_o. The voltage source resistance is R_o. We assume the stray inductance to be negligible compared with L_2. A similar circuit is frequently used to measured an unknown resistance R_o, through which a known external current is passed to generate the voltage V_o. The SQUID is again used as a null sensor, with current feedback to the standard resistor R_s. The open-loop time-constant of the circuit, $\tau = L_2/(R_o + R_s)$ is drastically reduced by feedback to a value τ_{FB}. When $L_2/(R_o + R_s)$ is the dominant time-constant in the open-loop circuit, Newbower[43] has shown that $\tau_{FB} = (L_2/GR_s + L_s/R_s)$, where G is the loop current gain, and L_s is the stray inductance associated with R_s (we assume all stray inductances $<< L_2$). Thus in the limit of very high loop gain, τ_{FB} becomes L_s/R_s, but in general τ_{FB} is dependent upon L_2. The response function of the feedback loop contains a term $(1 + j\omega\tau_{FB})^{-1}$. Thus the circuit responds to signals or noise at frequencies $\lesssim 1/2\pi\tau_{FB}$. We shall assume that the feedback current is measured in a bandwidth B set by a time-constant <u>outside</u> the feedback loop. The feedback also considerably

enhances the input impedance of the voltmeter: at zero frequency, it becomes approximately GR_s.

The SLUG[17] is used in a slightly different configuration. The voltage source and R_s are connected directly across the two ends of the Nb wire on which the SLUG is made [Fig. 1(f)]. The SLUG is again used as a null detector, with current feedback to R_s. Efficient transformers for use with higher impedance sources have also been developed.[44]

We turn now to a noise analysis of the voltmeter. We shall follow the general approach of Giffard et al.[30]; it should be noted however that these authors appear to have incorrectly used $(1 + j\omega\tau)^{-1}$ rather than $(1 + j\omega\tau_{FB})^{-1}$ in their response function. We assume that the bandwidth B in which the current noise is measured is small compared with $1/\tau_{FB}$. The action of the feedback circuit is to oppose any noise voltages appearing in the voltmeter circuit up to frequencies $\sim 1/2\pi\tau_{FB}$. However, the noise observed in the feedback current is restricted to the bandwidth B. The observed mean square Johnson noise generated in $(R_o + R_s)$ and referred to the voltmeter circuit is just $4kT(R_o + R_s)B$. The observed mean square flux noise due to the SQUID is equivalent to a mean square current noise $\alpha^2\Phi_o{}^2B/M^2$ in the voltmeter circuit, or to a mean square voltage noise $\alpha^2\Phi_o{}^2 (R_o + R_s)^2 B/M^2$. The total observed mean square voltage noise referred to the voltmeter circuit is therefore

$$\overline{E_N^2} = 4kT(R_o+R_s)B + \alpha^2\Phi_o{}^2(R_o+R_s)^2B/M^2. \qquad (29)$$

The mean square Johnson noise developed in the source resistance in a bandwidth B is just

$$\overline{E_{R_o}^2} = 4kTR_oB. \tag{30}$$

The noise factor[30] $F = \overline{E_N^2}/\overline{E_{R_o}^2}$ for the voltmeter is then:

$$F = \frac{R_o+R_s}{R_o} + \frac{\alpha^2\Phi_o^2 (R_o+R_s)^2}{4kTR_o\sigma^2LL_2}. \tag{31}$$

F is independent of B, as expected, provided that $B \ll 1/\tau_{FB}$. Now in practice, R_o can be made large compared with R_s, since the feedback enhances the input impedance to GR_s. If $R_o \gg R_s$, we can approximate Eq. (31) by

$$F \simeq 1 + \frac{\alpha^2\Phi_o^2R_o}{4kT\sigma^2LL_2}. \tag{32}$$

We define the noise temperature T_N of the voltmeter as the value of T for which F = 2, that is,

$$T_N = \frac{\alpha^2\Phi_o^2 R_o}{4k\sigma^2LL_2}. \tag{33}$$

Notice that for a given source resistance, the only variable parameter in Eq. (33) is L_2 (although in practice σ may decrease somewhat as L_2 is increased). Hence we may decrease the noise temperature by increasing the value of L_2, provided that τ_{FB} remains larger than 1/B. If B is made comparable to or larger than $1/\tau_{FB}$, Eqs. (29)-(33) are no longer valid. In practice, it is common to make $\tau \simeq L_2/R_o$ on the order of one second or less, although this value by no means represents an upper limit

on τ. If we insert the values $\alpha \sim 10^{-4}$, $\sigma \sim 0.8$, $L \sim 10^{-9}$H and $L_2/R_o \sim 1$ sec in Eq. (33) we find $T_N \sim 10^{-6}$K.

If the circuit is at a temperature T, the total mean square noise is less than or equal to twice the mean square noise in R_o (i.e. $F \leq 2$) if

$$\frac{L_2}{R_o} \geq \frac{\alpha^2 \Phi_o^2}{4k\sigma^2 LT} . \qquad (34)$$

For the values given above, $\alpha^2\Phi_o^2/4k\sigma^2 L \simeq 10^{-6}$K sec. This value has been used to plot R_o against L_2 for various temperatures in Fig. 12 (assuming $R_o >> R_s$). At a given temperature, F will be less than 2 if the values of R_o and L_2 lie to the left of the appropriate line. For small enough R_o and high enough T, it is possible to choose L_2 so that F is very close to unity, and the Johnson noise in R_o completely dominates the SQUID noise. Thus Giffard et al.[30] were able to use the noise in a 3μΩ resistor as a noise thermometer down to a few mK. For very low values of R_o, it is usual to make L_2 fairly small to reduce τ, but there is little point in making L_2 smaller than the stray circuit inductance, typically 10^{-8} to 10^{-7}H. However, values of τ greater than 100 sec have been used, the system time-constant, τ_{FB}, still being conveniently short. The upper limit on R_o for which $F \leq 2$ is set by the largest value of L_2 which can be tightly coupled to the SQUID. An inductance of 10^{-5}H would limit R_o to 40Ω [from Eq. (34)]. Higher values of L_2 could be used, but σ would probably be smaller. However, it appears that noise factors of $\lesssim 2$ can be achieved in the He^4 range for source resistances of up to several tens of Ohms. The noise power in a measurement limited

by Johnson noise is $4kTB$, about 6×10^{-23}W at 1K in a 1 Hz bandwidth. Measurements at this level of sensitivity are routinely made: For example, the rms noise voltage in a $10^{-8}\Omega$ resistor at 1K, about $8 \times 10^{-16}V/\sqrt{Hz}$, is readily observable.

Giffard et al.[30] have given a detailed specification of one of their voltmeters. With $R_o \sim 10^{-4}\Omega$, they achieved a total peak-to-peak noise and drift of about $4 \times 10^{-13}V/\sqrt{Hz}$ over a period of 5 min. This noise level is about three times the Johnson noise in R_o measured over a shorter period: presumably extraneous noise and/or electronic drift contributed significantly to the observed noise. The input impedance was about 4Ω, the maximum slewing rate better than $10^{-9}V\ sec^{-1}$ and the dynamic range 4×10^4. They estimated an upper limit on R_o of roughly 1Ω for $F \lesssim 2$.

In some applications, it might be desirable to modulate V_o (rather than the flux applied to the SQUID) at an audio frequency ($\ll 1/\tau_{FB}$). The amplitude of the alternating feedback current is then measured by a lock-in detector outside the feedback loop. The same noise analysis applies. An example of such an application would be when V_o arises from an infrared detector: it is usual to chop the incoming signal in order to remove the effects of unwanted background radiation.

All of the high resolution voltage measurements have been made inside superconducting shielding, and it seems likely that measurements will be restricted to voltages originating in a cryogenic environment. Examples of the use of the voltmeter (SLUG[17]) are in the measurement of thermoelectric emfs,[45] flux creep in superconductors,[46] and proximity effects in SNS sandwiches.[47] A SLUG was also used to compare the Josephson voltage-frequency relation [Eq. (5)] in different superconductors[48]

to a precision of 1 part in 10^8, and recently, to demonstrate that the quasiparticle potential differs from the pair potential in a non-equilibrium superconductor.[49]

V. SUMMARY

It is probably fair to state that the type of Josephson junction which is completely reproducible and reliable has yet to be developed. Nevertheless, present types of junction have proved very reliable in practice, and DC and RF SQUIDS have been used very satisfactorily in a number of laboratories for the past seven or eight years. During that time, most of the applications seem to have used the DC SQUID or SLUG , which of course preceeded the RF SQUID. However, most of the instruments currently being developed are based on RF SQUIDS, and these devices are now available commercially from at least two sources.[50] It seems likely that the RF SQUID will become the more popular, although the development of highly reliable and reproducible tunnel junctions may favour the DC SQUID.

The sensitivity of SQUIDS commonly used is 10^{-4} to $10^{-3}\Phi_o/\sqrt{Hz}$. Improvements upon this resolution have already been achieved, and it seems likely that a sensitivity of at least $10^{-5}\Phi_o/\sqrt{Hz}$ will eventually become available. SQUIDS, nearly always in conjunction with flux transformers, have been used to measure magnetic fields

(down to 10^{-14} T/$\sqrt{\text{Hz}}$), magnetic field gradients (down to 10^{-12} T/m/$\sqrt{\text{Hz}}$), and magnetic susceptibilities. A SQUID voltmeter can have a noise temperature as low as 10^{-6}K, and be limited by Johnson noise in the circuit resistance at liquid helium temperatures, provided the resistance is below a few tens of Ohms.

ACKNOWLEDGEMENTS

I am pleased to acknowledge helpful discussions with Professor M. R. Beasley, Dr. R. P. Giffard, Professor M. Tinkham, Dr. J. R. Waldram, and Dr. J. E. Zimmerman during the course of this work. I should like to thank the Roayl Society Mond Laboratory, Cambirdge, England, for its hospitality during the writing of this article.

This work was supported in part by the U. S. Atomic Energy Commission.

References and Footnotes.

* Alfred P. Sloan Foundation Fellow.

[1] B. D. Josephson, "Possible new effects in superconductive tunnelling", Phys. Letters, vol. 1, pp. 251-253, 1962; see also "Supercurrents through barriers", Adv. in Phys., vol. 14, pp. 419-451, 1965.

[2] For an elementary review and references, see J. Clarke, "The Josephson effect and e/h", Amer. J. Phys., vol. 38, pp. 1071-1095, 1970.

[3] J. Bardeen, L. N. Cooper, and J. R. Schrieffer, "Theory of superconductivity", Phys. Rev. vol. 108, pp. 1175-1204, 1957.

[4] F. London, Superfluids (Wiley, New York, 1950).

[5] B. S. Deaver and W. M. Fairbank, "Experimental evidence for quantized flux in superconducting cylinders", Phys. Rev. Letters vol. 7, pp. 43-46, 1961; R. Doll and M. Näbauer, "Experimental proof of magnetic flux quantization in a superconducting ring", Phys. Rev. Letters vol. 7, pp. 51-52, 1961.

[6] P. W. Anderson, "Special effects in superconductivity", in Lectures on the many body problem , Ravello, edited E. R. Caianiello (Academic, New York, 1964), vol. 2, pp. 113-135.

[7] P. W. Anderson and J. M. Rowell, "Probable observation of the Josephson superconducting tunnelling effect," Phys. Rev. Letters, vol. 10, pp. 230-232, 1963.

[8] For a review, see W. Schroen, "Physics of preparation of Josephson barriers", J. Appl. Phys., vol. 39, pp. 2671-2678, 1968.

[9] J. E. Nordman, "Thin-film Josephson junctions using getter-sputtered niobium", J. Appl. Phys., vol. 40, pp. 2111-2115, 1969; L. O. Mullen and D. B. Sullivan, "Fabrication of tunnel junctions on niobium films",

J. Appl. Phys., vol. 40, pp. 2115-2117, 1969; R. Graeffe and T. Wiik, "Preparation of Josephson junctions by plasma oxidation of Nb", J. Appl. Phys., vol. 42, pp. 2146-2147, 1971; K. Schwidtal, "Dc and ac Josephson effect in sputtered Nb-NbOx-Pb junctions", J. Appl. Phys., vol. 43, pp. 202-208, 1972.

[10] J. Clarke, "Supercurrents in lead-copper-lead sandwiches", Proc. Roy. Soc., vol. A308, pp. 447-471, 1969.

[11] P. W. Anderson and A. H. Dayem, "Radio-frequency effects in superconducting thin film bridges", Phys. Rev. Letters, vol. 13, pp. 195-197, 1964.

[12] F. Considori, A. A. Fife, R. F. Frindt, and S. Gygax, "Construction and properties of weak-link detectors using superconducting layer structures", Appl. Phys. Letters, vol. 18, pp. 233-235, 1971.

[13] H. A. Notarys, R. H. Wang, and J. E. Mercereau, "Weakly superconducting circuits", Proc. IEEE, (this issue).

[14] J. E. Mercereau, "Superconducting magnetometers", Rev. de Phys. Appl. vol. 5, pp. 13-20, 1970; M. Nisenoff, "Superconducting magnetometers with sensitivities approaching 10^{-10} gauss", Rev. de Phys. Appl., vol. 5, pp. 21-24, 1970; H. A. Notarys and J. E. Mercereau, "Dynamics of small superconductors", Proceedings of the International Conference on the Science of Superconductivity, Stanford, U.S.A., 26-29 August 1969 (Ed. F. Chilton) pp. 424-431.

[15] J. E. Zimmerman and A. H. Silver, "Macroscopic quantum interference effects through superconducting point contacts", Phys. Rev. vol. 141, pp. 367-375, 1966.

[16] R. A. Buhrman, S. F. Strait, and W. W. Webb, "Stable superconducting point-contact weak links", J. Appl. Phys., vol. 42, pp. 4527-4528, 1971.

[17] J. Clarke, "A superconducting galvanometer employing Josephson tunnelling", Phil. Mag., vol. 13, pp. 115-127, 1966.

[18] T. A. Fulton and R. C. Dynes, "Current-phase relations in superconducting bridges", Phys. Rev. Letters, vol. 25, pp. 794-797, 1970; P. E. Gregers-Hansen, M. T. Levinsen, and G. Fog Pedersen, "A sinusoidal current-phase relation for superconducting thin-film microbridges", J. Low Temp. Phys., vol. 7, pp. 99-118, 1972.

[19] W. C. Stewart, "Current-voltage characteristics of Josephson junctions", Appl. Phys. Letters, vol. 12, pp. 277-280, 1968; D. E. McCumber, "Effect of ac impedance on dc voltage-current characteristics of superconductor weak-link junctions", J. Appl. Phys., vol. 39, pp. 3113-3118, 1968.

[20] P. K. Hansma, G. I. Rochlin, and J. N. Sweet, "Externally shunted Josephson junctions: generalized weak links", Phys. Rev., vol. 4B, pp. 3003-3014, 1971.

[21] R. de Bruyn Ouboter and A. Th. A. M. de Waele, "Superconducting point contacts weakly connecting two superconductors", Progress in Low Temperature Physics (Ed. C. J. Gorter, North-Holland, Amsterdam-London, 1970), vol. VI, pp. 243-290.

[22] W. W. Webb, "Superconducting quantum magnetometers", IEEE Transactions on Magnetics, vol. MAG-8, pp. 51-60, 1972.

[23] R. C. Jaklevic, J. Lambe, A. H. Silver, and J. E. Mercereau, "Quantum interference effects in Josephson tunnelling", Phys. Rev. Letters, vol. 12, pp. 159-160, 1964.

[24] J. Clarke and J. L. Paterson, "Josephson-junction amplifier", Appl. Phys. Letters, vol. 19, pp. 469-471, 1971.

[25] M. R. Beasley and W. W. Webb, "Operation of superconducting interference devices in appreciable magnetic fields", Proceedings of the Symposium on the Physics of Superconducting Devices, April 28-29, 1967, University of Virginia, Charlottesville, pp. V-1 - V-8.

[26] P. L. Forgacs and A. Warnick, "Digital-analog magnetometer utilizing superconducting sensor", Rev. Sci. Instr., vol. 38, pp. 214-220, 1967.

[27] R. K. Kirschman and J. E. Mercereau ("Current noise in weak superconductors," Phys. Letters, vol. 35A, pp. 177-178, 1971) showed that for a current-biased junction of the type shown in Fig. 1(d) the total noise developed was Nyquist noise in a bandwidth $RI_c/4\Phi_o$. We assume that in an externally limited bandwidth B, the junction noise is just Nyquist noise in the bandwidth B.

[28] J. E. Zimmerman, P. Thiene, and J. T. Harding, "Design and operation of stable rf-biased superconducting point-contact quantum devices, and a note on the properties of perfectly clean metal contacts", J. Appl. Phys., vol. 41, pp. 1572-1580, 1970.

[29] J. M. Goodkind and D. L. Stolfa, "The superconducting magnetic flux detector", Rev. Sci. Instr., vol. 41, pp. 799-807, 1970.

[30] R. P. Giffard, R. A. Webb, and J. C. Wheatley, "Principles and methods of low-frequency electric and magnetic measurements using an rf-biased point-contact superconducting device", J. Low Temp. Phys., vol. 6, pp. 533-610, 1972.

[31] J. E. Zimmerman, "Josephson effect devices and low-frequency field sensing", Cryogenics, vol. 12, pp. 19-31, 1972.

[32] M. B. Simmonds and W. H. Parker, "Analog computer simulation of weakly connected superconducting rings", J. Appl. Phys., vol. 42, pp. 38-45, 1971.

[33] If the junction inductance is properly taken into account (for example, ref. 22), this criterion becomes $LI_c < \Phi_o/2\pi$. Simmonds and Parker (ref. 32) showed that the results of the two models are remarkably similar for $LI_c \gtrsim \Phi_o/2$.

[34] J. Kurkijärvi, "Intrinsic fluctuations in a superconducting ring closed with a Josephson junction', Phys. Rev., vol. 6B, pp. 832-835, 1972; J. Kurkijärvi and W. W. Webb, "Thermal fluctuation noise in a superconducting flux detector", to be published in the Proceedings of the Applied Superconductivity Conference, Annapolis, Maryland, May 1-3, 1972.

[35] J. M. Goodkind and J. M. Dundon, "New fabrication of superconducting flux detector", Rev. Sci. Instr., vol. 42, pp. 1264-1265, 1971.

[36] J. E. Zimmerman and N. W. Frederick, "Miniature ultrasensitive superconducting magnetic gradiometer and its use in cardiography and other applications", Appl. Phys. Letters, vol. 19, pp. 16-19, 1971.

[37] R. A. Kamper and M. B. Simmonds, "Broadband Superconducting Quantum Magnetometer", Appl. Phys. Letters, vol. 20, pp. 270-272, 1972.

[38] J. E. Zimmerman, "Sensitivity enhancement of superconducting quantum interference devices thorugh the use of fractional turn loops", J. Appl. Phys., vol. 42, pp. 4483-4488, 1971.

[39] J. E. Lukens, R. J. Warburton, and W. W. Webb, "Versatile superconducting femtovoltmeter amplifier and multimeter", J. Appl. Phys., vol. 42, pp. 27-30, 1971.

[40] J. P. Gollub, M. R. Beasley, R. S. Newbower, and M. Tinkham, "Observation of enhanced diamagnetism above T_c in indium due to thermodynamic fluctuations", Phys. Rev. Letters, vol. 22, pp. 1288-1291, 1969.

[41] J. E. Lukens, R. J. Warburton, and W. W. Webb, "Onset of quantized thermal fluctuations in 'one dimensional' superconductors", Phys. Rev. Letters, vol. 25, pp. 1180-1184, 1970.

[42] H. E. Hoenig, R. H. Wang, G. R. Rossman, and J. E. Mercereau, "Magneto-chemical studies with a new ultrasensitive superconducting quantum magnetometer", to be published in the Proceedings of the Applied Superconductivity Conference, Annapolis, Maryland, May 1-3, 1972.

[43] R. S. Newbower, "Femtovolt measurements of the superconducting transition in tin whisker crystals", Ph.D. thesis, Harvard University, January 1971 (published as a technical report by the Office of Naval Research).

[44] J. Clarke, W. E. Tennant, and D. Woody, "Impedance matching a Josephson galvanometer by means of a superconducting transformer", J. Appl. Phys., vol. 42, pp. 3859-3865, 1971.

[45] E. Rumbo, "Measurement of thermoelectric power at low temperatures", Phil. Mag., vol. 19, pp. 689-691, 1969.

[46] M. Wade, "Evidence against thermal activation as the cause of flux creep in type II superconductors", Phil. Mag., vol. 20, pp. 1107-1114, 1969.

[47] A. B. Pippard, J. G. Shepherd and D. A. Tindall, "Resistance of superconducting-normal interfaces", Proc. Roy. Soc., vol. A324, pp. 17-35, 1971.

[48] J. Clarke, "Experimental comparison of the Josephson voltage-frequency relation in different superconductors", Phys. Rev. Letters, vol. 21, pp. 1566-1569, 1968.

[49] J. Clarke, "Experimental observation of pair-quasiparticle potential difference in non-equilibrium superconductors", Phys. Rev. Letters, vol. 28, pp. 1363-1366, 1972.

[50] Develco, Inc., Mountain View, California; and S.H.E. Corporation, La Jolla, California.

Figure Captions.

1. Types of Josephson junction. Typical dimensions are indicated. (a) Superconductor - oxide - superconductor tunnel junction; (b) Pb-Cu-Pb junction; (c) Anderson-Dayem bridge; (d) Notarys bridge with normal metal underlay; (e) point contact; (f) SLUG.

2. (a) Model of Josephson junction: the tunnelling element (J) is in parallel with a resistance R. (b) I-V characteristic of the model shown in (a).

3. (a) Two junctions (×) mounted on superconducting ring; (b) I_c as function of external flux Φ_e; (c) I-V characteristics for $\Phi_e = n\Phi_o, (n+1/2)\Phi_o$; (d) circulating current (j) as function of Φ_e.

4. Practical DC SQUIDS: (a) made from split Nb cylinder; (b) made from Nb foil.

5. DC SQUID feedback system.

6. Basic detection circuit for RF SQUID, mounted in the cryostat. R_T is the resistance of the tank coil.

7. Flux enclosed in RF SQUID (Φ_s) as a function of an external flux (Φ_e) swept from 0 to $3\Phi_o$; to $-3\Phi_o$, and to Φ_o.

8. V_T versus i_d for RF SQUID; both V_T and i_d are peak values.

9. Types of RF SQUIDS: (a) single hole device made from Nb cylinder; (b) double hole device, also made from Nb cylinder; (c) thin film evaporated on to a quartz rod.

10. RF SQUID feedback system.

11. (a) Rudimentary flux transformer; (b) and (c) gradiometers.

12. Plots of $R_o = 10^6 L_2 T$ for five temperatures. If the values of R_o and L_2 lie to the left of the line appropriate to the given temperature, the noise factor of the voltmeter is less than 2.

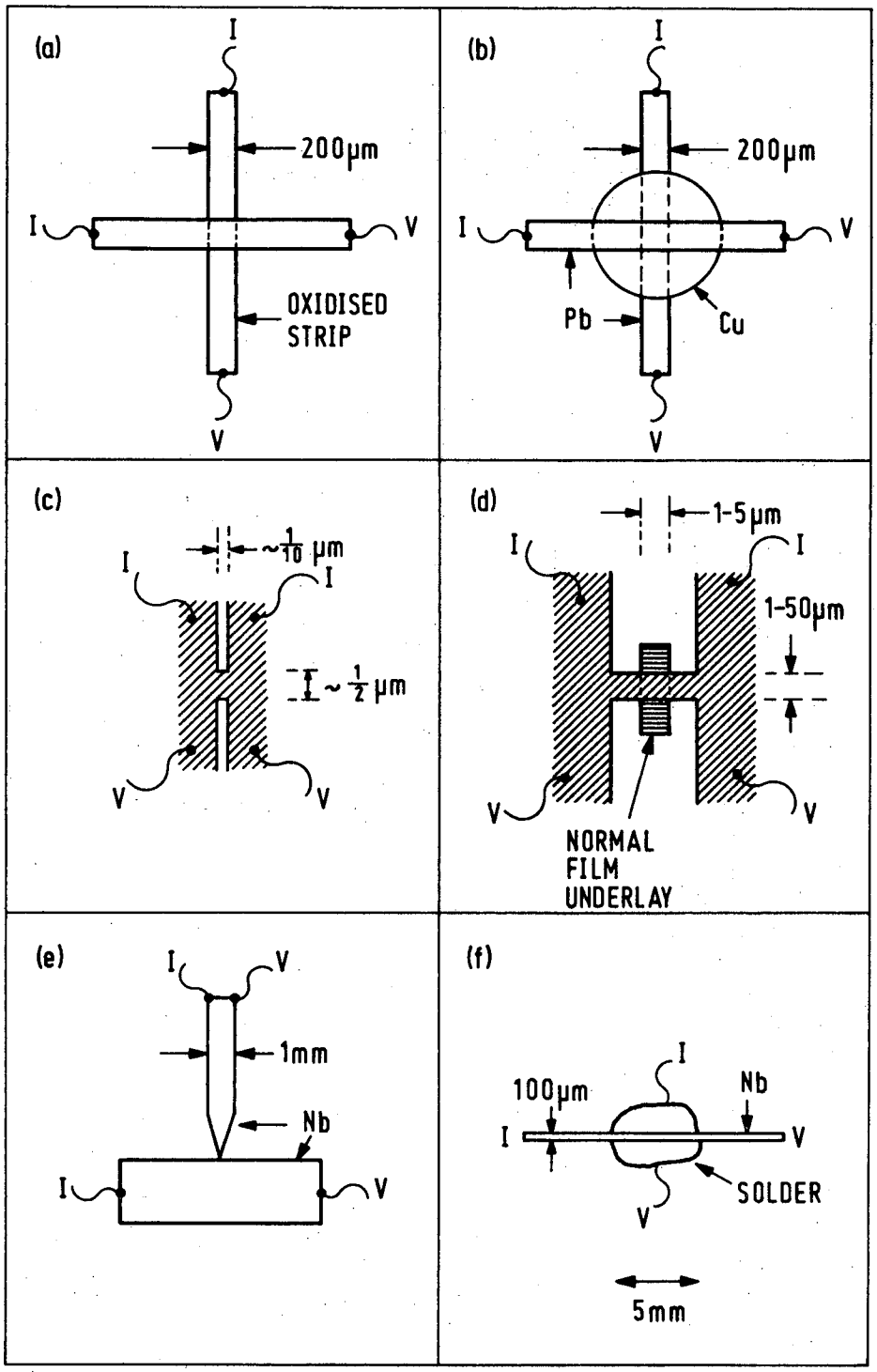

XBL 727-6609

Fig. 1

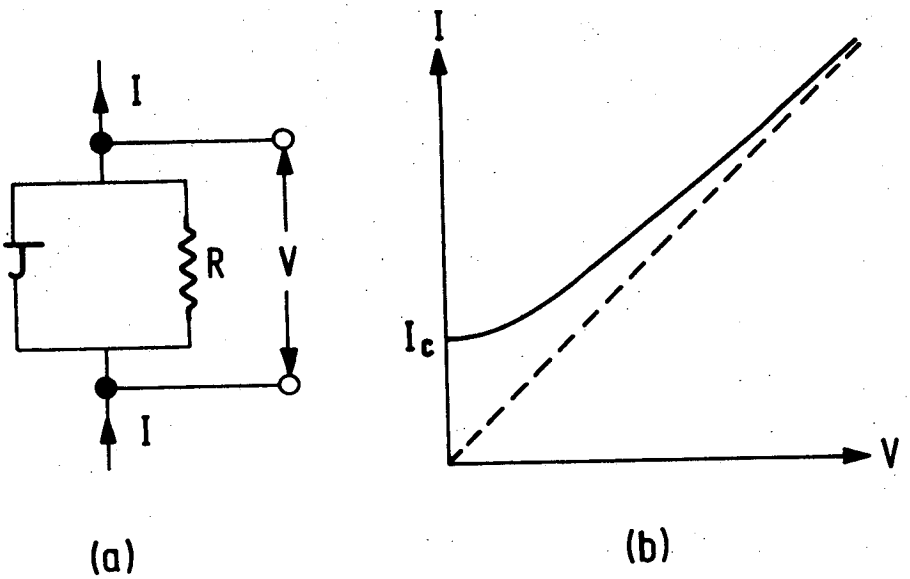

XBL 727-6610

Fig. 2

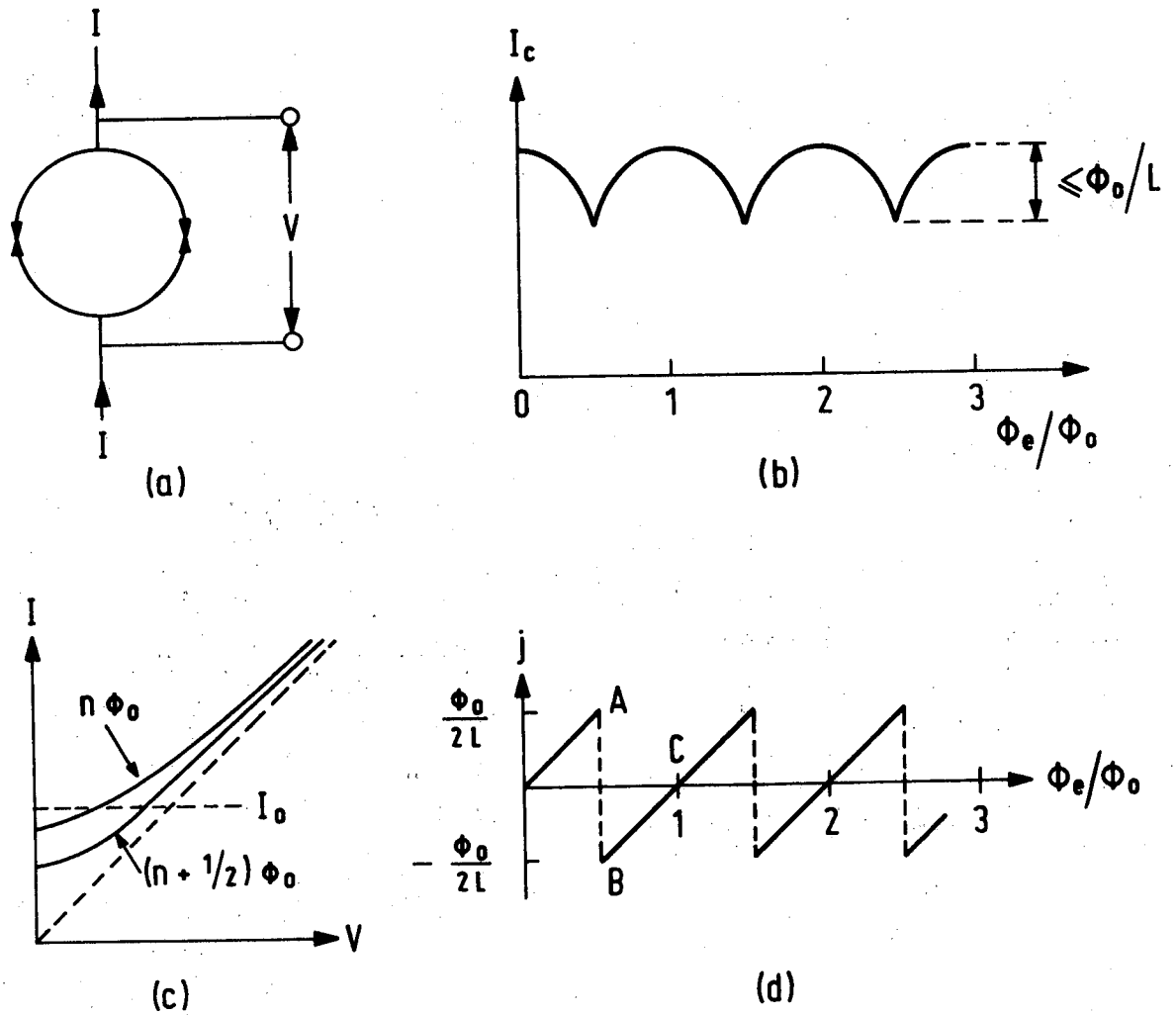

XBL 727-6611

Fig. 3

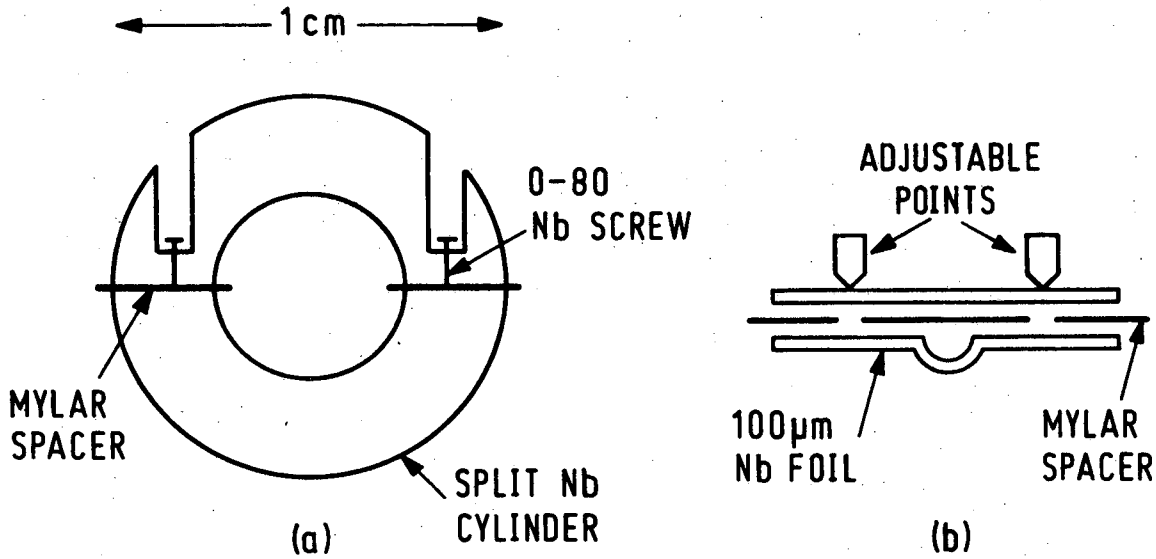

XBL 727-6612

Fig. 4

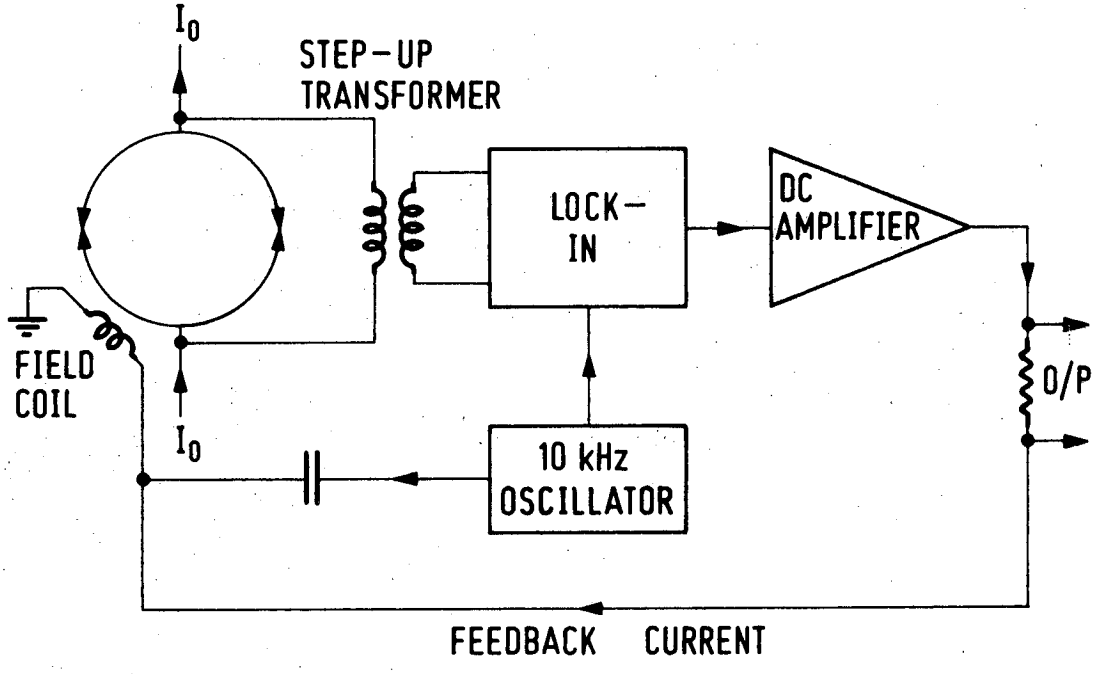

XBL 727-6613

Fig. 5

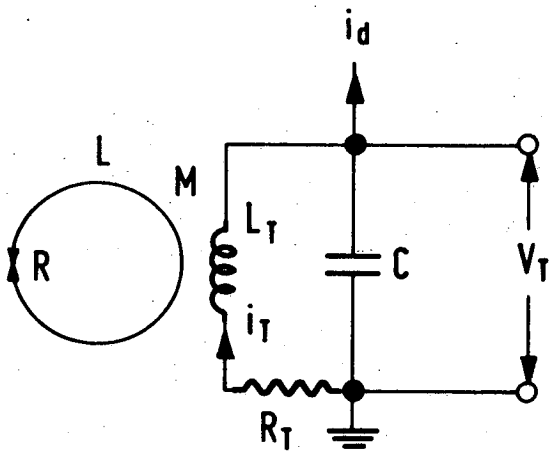

XBL 727-6614

Fig. 6

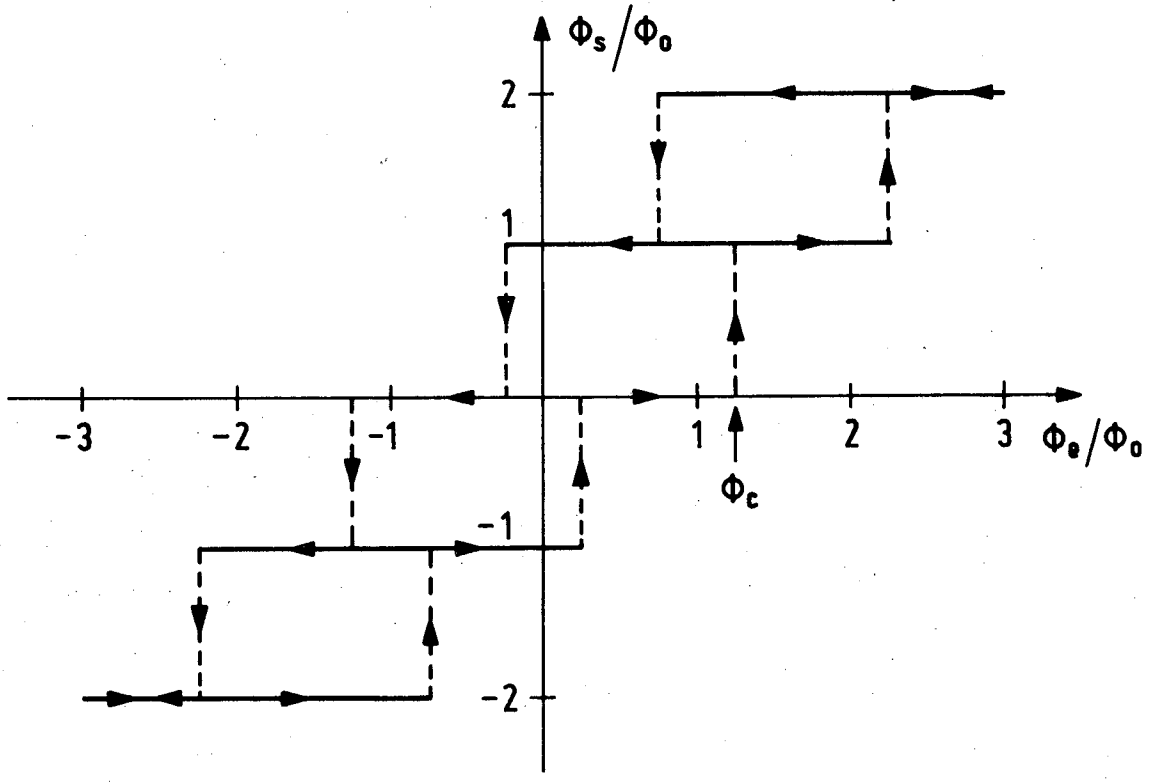

XBL 727-6615

Fig. 7

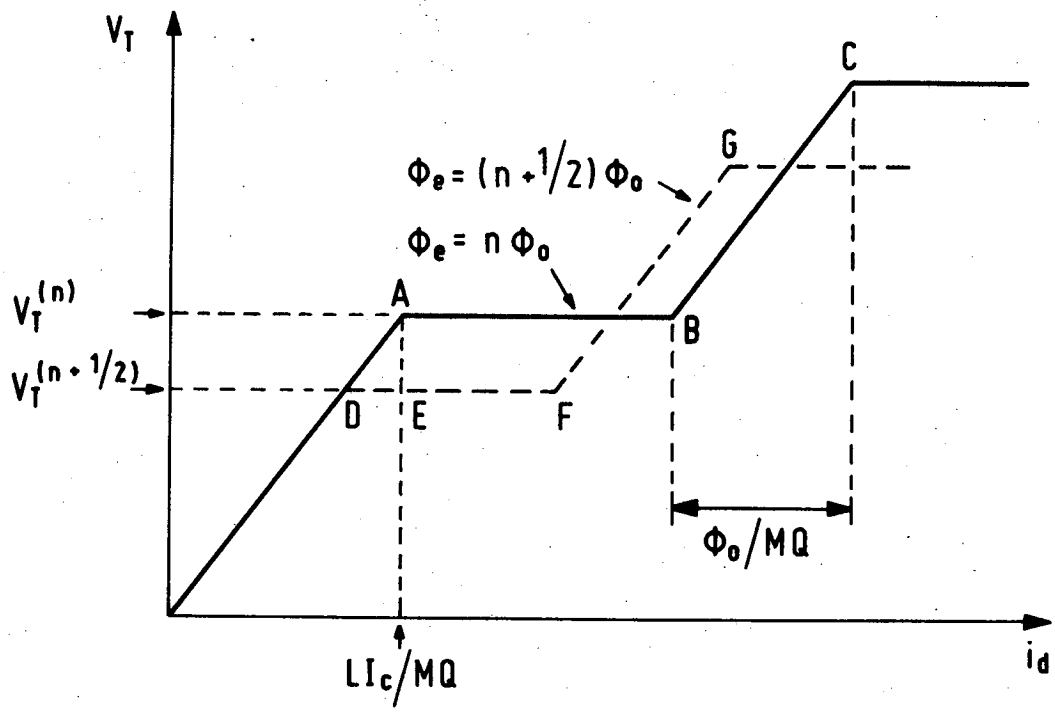

XBL 727-6616

Fig. 8

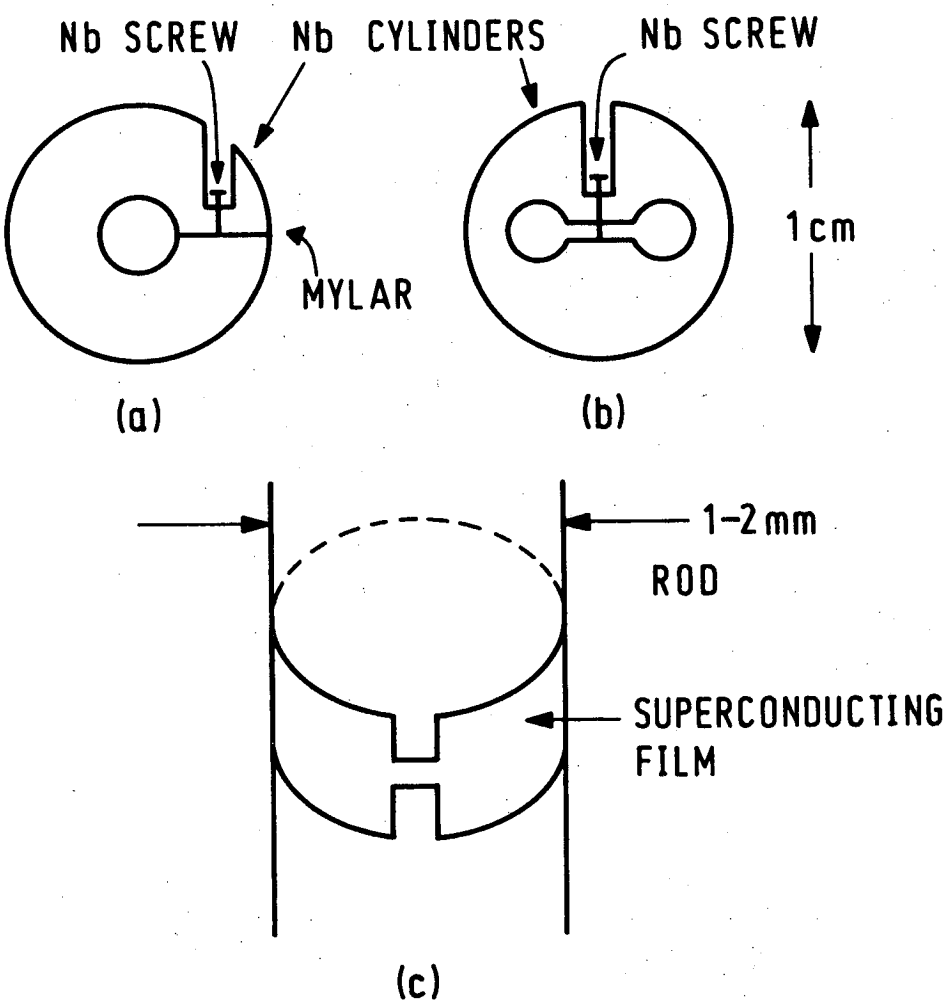

XBL 727-6617

Fig. 9

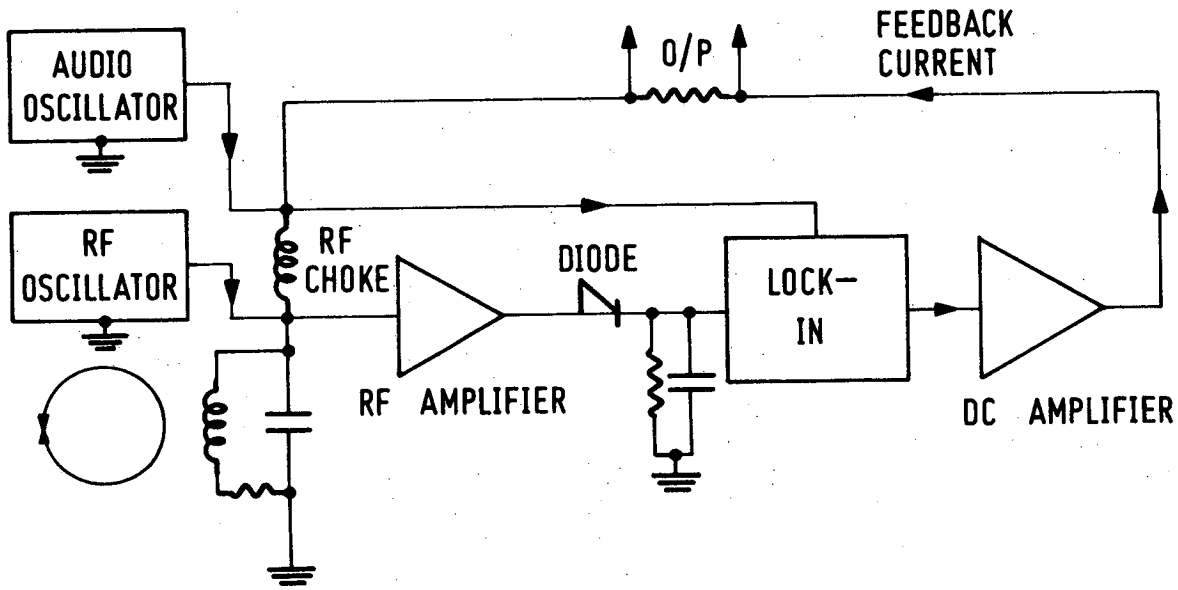

XBL 727-6618

Fig. 10

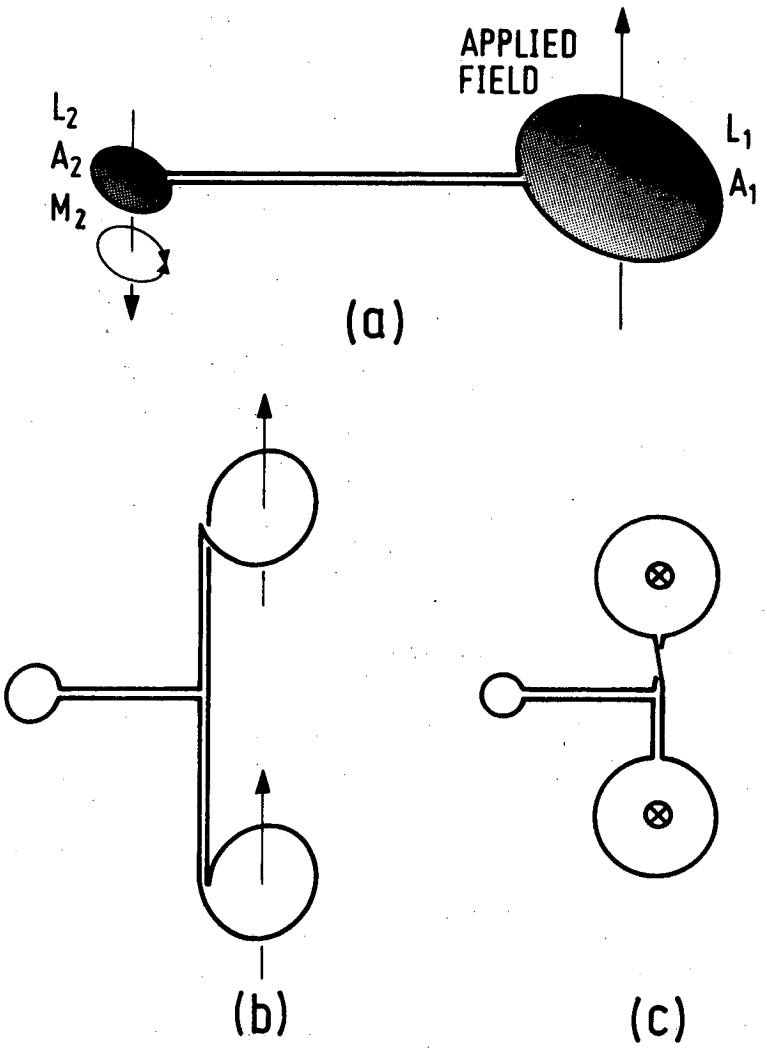

XBL 727-6619

Fig. 11

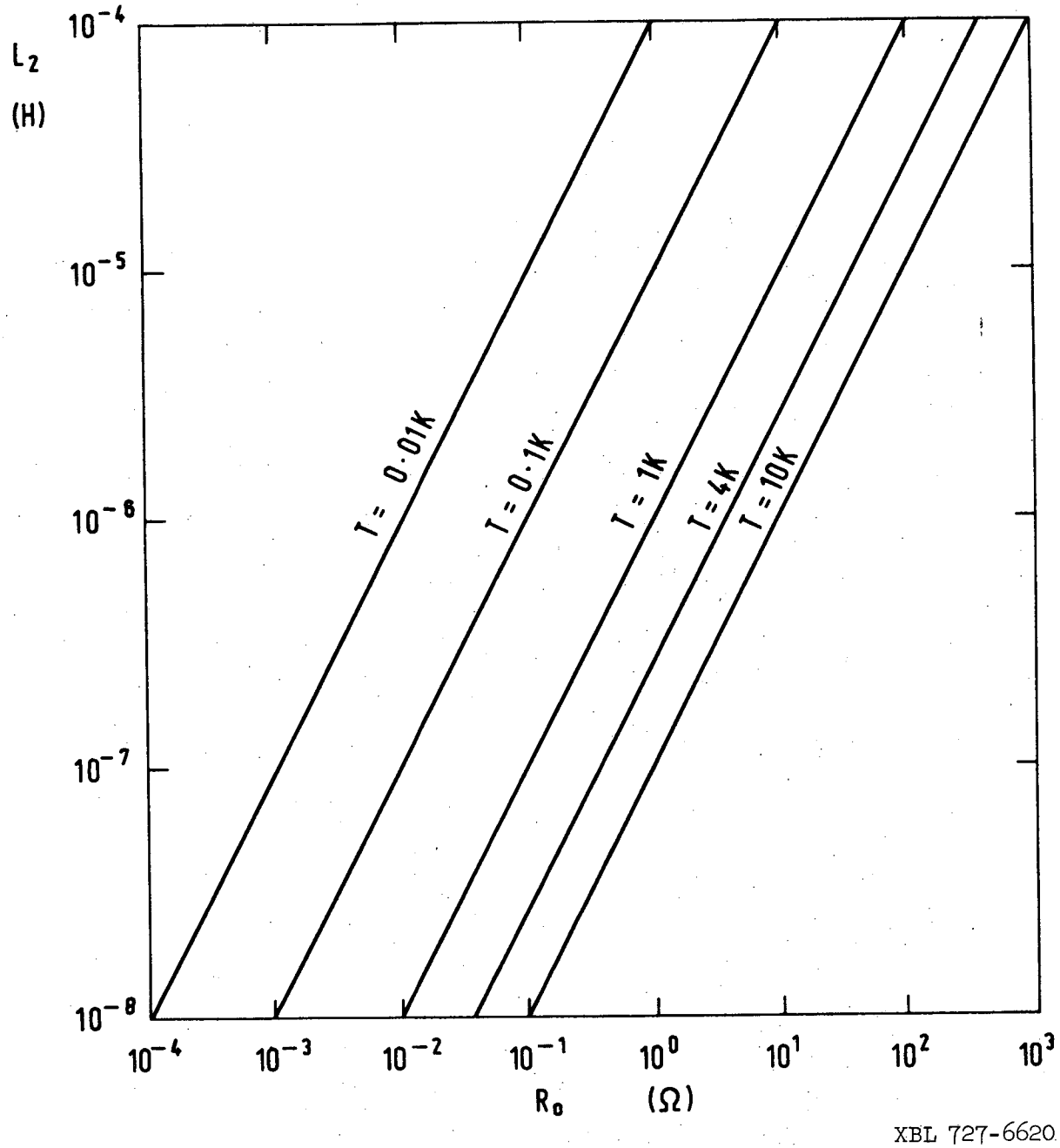
L_2
(H)
10^{-4}
10^{-5}
10^{-6}
10^{-7}
10^{-8}
T = 0·01K
T = 0·1K
T = 1K
T = 4K
T = 10K
10^{-4}
10^{-3}
10^{-2}
10^{-1}
10^{0}
10^{1}
10^{2}
10^{3}
R_0 (Ω)
XBL 727-6620

Fig. 12

TECHNICAL INFORMATION DIVISION
LAWRENCE BERKELEY LABORATORY
UNIVERSITY OF CALIFORNIA
BERKELEY, CALIFORNIA 94720